Astron. Astrophys. 325, 81–97 (1997)

ASTRONOMY
AND
ASTROPHYSICS

Circumnuclear molecular gas and star formation in starburst galaxies

P. Planesas[1], **L. Colina**[2,⋆], **and D. Pérez-Olea**[2,3]

[1] Observatorio Astronómico Nacional (IGN), Apartado 1143, E-28800 Alcalá de Henares, Spain
[2] Space Telescope Science Institute, 3700 San Martin Drive, Baltimore, MD 21218, USA
[3] Departamento de Física Teórica, Módulo C-XI, Universidad Autónoma de Madrid, Cantoblanco, E-28049 Madrid, Spain

Received 18 April 1996 / Accepted 10 March 1997

Abstract. The molecular gas properties and circumnuclear star formation in the nearby nuclear starburst galaxies NGC 2903, NGC 3351 and NGC 3504 are investigated in detail. The circumnuclear HII regions in the star-forming rings of these galaxies are characterised by an ionized gas mass in the $10^4 - 10^5$ $M_\odot$ range, and by an ionizing flux in the $10^{51} - 10^{52}$ ph s^{-1} range, typical of giant HII regions in external galaxies.

The CO 2→1 emission in NGC 3504 indicates the presence of two emitting regions separated by 115 km s^{-1} in velocity and 5″ (500 pc) spatially, what approximately corresponds to the location of the the inner inner Lindblad resonance. The measured (CO 2→1)/(CO 1→0) integrated intensity ratio for the inner kpc of NGC 3351 is 0.8, in agreement with the empirical average value found for spiral galaxies with a normal metallicity regardless of the presence or the absence of a starburst.

Molecular gas masses in the range of $M_{H_2} \approx 10^8 - 10^9$ $M_\odot$ are measured in regions of a few hundred parsecs in size. On average, the circumnuclear region of the three galaxies is characterised by an average molecular gas surface density Σ_{H_2} = 280 $M_\odot$ pc^{-2}, and average L_{IR}/M_{H_2}= 21 $L_\odot$ $M_\odot{}^{-1}$.

The $L_{IR}/M_{H_2} - \Sigma_{H_2}$ relationship covering the Σ_{H_2} range from normal spiral galaxies and giant molecular clouds in the Milky Way with $\Sigma_{H_2} \sim 10^1 - 10^2$ $M_\odot$ pc^{-2}, to nearby starbursts, AGNs with starbursts, and luminous IRAS galaxies with $\Sigma_{H_2} \sim 2\ 10^2 - 10^5$ $M_\odot$ pc^{-2}, is investigated. Nearby starburst galaxies have an average molecular gas surface density Σ_{H_2} of 400 $M_\odot$ pc^{-2} and an average L_{IR}/M_{H_2} of 23 $L_\odot$ $M_\odot{}^{-1}$. These two properties are explained by the existence of giant molecular clouds with associated HII regions where the star formation process is characterised by being short lived ($\leq 3\ 10^7$ years), biased towards a high lower mass limit $M_l \sim 3$ $M_\odot$, and with an overall gas to stars conversion fraction of $\leq 10\%$ of the gas mass.

The star formation efficiency (SFE) in nearby starbursts and luminous IRAS galaxies (as measured by the L_{IR}/M_{H_2} ratio) does not show any indication of a linear correlation with increasing Σ_{H_2}. On the contrary, the star formation efficiency is restricted to the $10 < L_{IR}/M_{H_2} < 100$ $L_\odot$ $M_\odot{}^{-1}$ range, and reaches a maximum value of L_{IR}/M_{H_2}= 100 $L_\odot$ $M_\odot{}^{-1}$ for Σ_{H_2} larger than 10^3 $M_\odot$ pc^{-2}. The upper limit found for the L_{IR}/M_{H_2} ratio, independent of Σ_{H_2}, implies the existence of an upper limit in the fraction of gas converted into stars independent of the density.

The SFE range observed in nearby starbursts, Seyferts with starbursts, and luminous IRAS galaxies is explained as a combination of massive star formation in the circumnuclear regions of these galaxies plus the additional contribution of an AGN at the center of the galaxy. Under the starburst+AGN scenario, most of the molecular gas mass is directly involved in the star forming process while the AGN contribution to the global IR luminosity is in the 10% to 75% range, depending on the galaxy. In this scenario, the infrared luminosity of galaxies with observed L_{IR}/M_{H_2} ratio in the 10 to 30 $L_\odot$ $M_\odot{}^{-1}$ range is dominated by the circumnuclear star formation alone. The infrared luminosity in those galaxies with L_{IR}/M_{H_2} in the 30–100 $L_\odot$ $M_\odot{}^{-1}$ range is increasingly dominated by the central AGN. Examples of this situation are NGC 1068, NGC 7469 and Mrk 231.

Key words: galaxies: general – galaxies: ISM – galaxies: Seyfert – galaxies: starburst

1. Introduction

In recent years, it has become apparent that enhanced star formation in the central regions of galaxies may be linked to the formation and fueling of a powerful active galactic nucleus (AGN) as such believed to exist in Seyfert galaxies, QSOs and in some luminous infrared galaxies (see review in Heckman 1991). Both the starburst and the AGN phenomenon could be promoted by an abundant supply of interstellar gas which would sustain a high star formation rate and feed a central black hole. Because the lifetimes of these phenomena are short and they are seen in

⋆ On assignment from the Space Science Department of ESA

otherwise old galaxies, it is unlikely that such activity is produced as a normal, albeit transient, phase in the life cycle of a normal galaxy. Mechanisms such as galaxy-galaxy interactions and mergers between spiral galaxies can provide the way for transporting the gas to the center of the host galaxy (Hernquist 1989; Barnes & Hernquist 1991). In a more gradual way, the non-axisymmetric gravitational potential of a central stellar bar can raise the rate at which the gas accretes to the galactic center (Noguchi 1988). Circumnuclear star forming rings expected to form around the inner Lindblad resonance region as consequence of the increase in gas density (Combes 1991) have been observed in a number of galaxies with a stellar bar (Telesco, Dressel & Wolstencroft 1993; Buta & Crocker 1993), while star formation appears concentrated in the nucleus when the galaxy has no bar (Telesco, Dressel & Wolstencroft 1993). However, it is clear that since a large fraction of both interacting and barred spiral galaxies show no evidence of either AGN or starburst activity, any kind of gravitational perturbation is not sufficient for these phenomena to occur. The existence of an abundant gas supply is certainly necessary for the starburst and may also be necessary, at least in the early phases, for the AGN.

Studies of the distribution of the molecular gas and star-forming regions in galaxies that harbor either a starburst or both a starburst and an AGN can provide clues on the nature of the mechanisms triggering the nuclear activity, as well as to help to establish the link between the two phenomena, starburst and AGN. In particular, it has been suggested that Seyferts need a higher concentration of molecular gas in the nucleus in order to feed the AGN before the gas is consumed by the starburst (Taniguchi, Nakai & Kameya 1991).

In the last few years surveys of molecular gas in Seyfert galaxies have been published (Heckman et al. 1989; Taniguchi, Nakai & Kameya 1991). The linear resolution in these surveys is in the range 2-20 kpc, hence only in a very few cases the circumnuclear gas concentration could be measured. The tentative conclusions were that there is no significant difference in the circumnuclear molecular gas surface density between Seyferts and starburst galaxies, and that the molecular gas in Seyferts is less concentrated toward the nuclear zones (Taniguchi, Nakai & Kameya 1991). Also, type 2 Seyferts have higher molecular gas content and star formation rates than type 1 Seyferts (Heckman et al. 1989).

Although the above quoted studies of CO emission give information about the total molecular gas content of Seyfert and starburst galaxies, the low angular resolution of the observations makes them inadequate to draw firm conclusions about the molecular gas distribution, the surface density, and the star formation efficiency in the circumnuclear regions of these galaxies.

On the other hand, luminous IRAS galaxies constitute the only group of galaxies for which high resolution CO observations, mostly with the Owens Valley millimeter interferometer, has been performed (Scoville et al. 1991 and references therein). Luminous IR galaxies are special when compared with other starburst galaxies in the large amount of molecular gas involved in the starburst (Scoville et al. 1991). However, there is observational evidence that the high efficiency of star formation in luminous IR galaxies is better traced by a high surface density of molecular gas than by a high total gas content (Scoville et al. 1991; Planesas, Mirabel & Sanders 1991). This is consistent with the most likely driving mechanism for high mass star formation, namely cloud-cloud collisions (Scoville, Sanders & Clemens 1986; see also review by Elmegreen 1994). Thus, a similar behaviour in the efficiency of star formation in other starburst galaxies that are less extreme in their content of molecular gas is expected.

A better understanding of the conditions that led to a starburst and/or an AGN, and of the way the starburst proceeds, can only be obtained from the detailed study of the molecular gas content and physical conditions in the circumnuclear zone, and the comparison with massive star formation as can be inferred from Hα images.

Sect. 2 of this paper is dedicated to explain the CO and optical observations of NGC 2903, NGC 3351 and NGC 3504 as well as the basic reduction procedure. Sects. 3 and 4 are devoted to the analysis of the CO and Hα maps, respectively. The characterization of the circumnuclear star forming regions is presented in Sect. 5, while a discussion of the observed star formation efficiency versus molecular surface density relation in nearby starbursts, Seyferts with starburst, and luminous IRAS galaxies is presented in Sect. 6.

2. Observations

NGC 3351 is a hot-spot galaxy (Sersic & Pastoriza 1967) harboring high-mass star formation in the nuclear region and in a ring 20″ in diameter (Alloin & Nieto 1982), the nuclear region having much larger surface density of high-mass stars than the ring (Devereux et al 1992). A more spectacular example of star formation in a hot-spot galaxy is NGC 2903. The large infrared luminosities and radio continuum emission clearly indicate the presence of a nuclear starburst (Wynn-Williams & Becklin 1985). NGC 3504 in the brightest galaxy in the optically selected catalog of starburst galactic nuclei in Balzano (1983). The three galaxies can be considered examples of nuclear starburst galaxies, in the sense that the star formation rate per unit area (as estimated from Hα emission) in the nuclear region is significantly enhanced when compared to the disk (cf. Sect. 4.6 in Jackson et al 1991 for NGC 2903, Sect. 4.3 in Devereux et al 1992 for NGC 3351, and Sect. 3.1 in Kenney et al 1993 for NGC 3504).

2.1. CO observations

CO J=2→1 and J=1→0 observations were made with the IRAM 30 m telescope at Pico de Veleta (Spain) on October 1991 and June 1992. The adopted parameters of the observed galaxies can be found in Table 1. The observing dates and the relevant telescope parameters can be found in Table 2a. We fully mapped (6″ steps) a region approximately 30″ × 30″ in size centered on the nucleus of each galaxy in the CO 2→1 transition (230 GHz). A CO 1→0 map was also obtained for NGC 3351.

Table 1. Adopted characteristics of the observed galaxies

Parameter	NGC 2903	NGC 3351	NGC 3504
Position of the nucleus			
α(1950)	$09^h29^m20^s.3$	$10^h41^m19^s.6$	$11^h00^m28^s.5$
δ(1950)	$21°43'21''$	$11°58'00''$	$28°14'32''$
Radial velocity (LSR)[a]	543	776	1544
Radial velocity (hel)[a]	550	782	1551
Distance (Mpc)[b]	7.3	10.4	20.7
Linear scale (pc/$''$)	35	51	100
Morphological type[c]	Sc(s)I-II	SBb(r)II	SBb(s)
Position angle	17°([d])	11°([e])	149°([d])
Inclination	60°([f])	46°([e])	22°([d])
B_T^d	9.7	10.5	11.7
$(B-V)_T^d$	0.7	0.8	0.7
L_{FIR} (10^9 $L_\odot$)[g]	3.7	3.4	13.7
L_{IR} (10^9 $L_\odot$)[h]	6.0	6.0	28.1
T_{dust} [i]	29	35	38

(a) Centroid of the CO emission
(b) Derived from the measured V_{hel}, and assuming $H_\circ$=75 km s^{-1} Mpc^{-1}
(c) From Sandage and Tammann, 1987
(d) From de Vaucouleurs et al. 1991
(e) Grosbol, 1985
(f) Jackson et al. 1989
(g) L_{FIR} = L($40-120\mu$m) calculated using prescription in Fullmer & Lonsdale 1989
(h) L_{IR} = L($8-1000\mu$m) calculated using prescription in Perault 1987 and the *IRAS* PSC fluxes
(i) from the S_{60}/S_{100} flux ratio and a λ^{-1} dust emissivity law.

The spectrometers used were 512 channel×1 MHz filter banks, which provided a velocity coverage wide enough, even at the highest frequency, and a velocity resolution of 1.3 km s^{-1} at 230 GHz and 2.6 km s^{-1} at 115 GHz. The focus of each receiver was checked every few hours, and corrections were applied when necessary. Such monitoring was more frequent around sunset and sunrise. Pointing was checked every 1-2 hours, and it was never found an error larger than $3''$. The corresponding galaxy central position was observed frequently in order to detect pointing changes through variations in the profile shape.

All observations were done in fast beam switching mode by nutating the subreflector at a rate of 1 Hz, with the reference position $4'$ away in azimuth, in order to obtain flat baselines. Linear baselines were subtracted from each spectrum. The calibrations were done by the chopper wheel method. Spectra toward Orion A and W51 at the redshifted frequencies were taken to obtain the absolute calibration for the temperature scale, using the IRAM 30m catalog of calibrated molecular lines. The temperature scale quoted in text and figures corresponds to T_{mb}, main beam brightness temperature corrected for atmospheric attenuation and rear spillover.

Table 2. Journal of the CO observations

Transition	CO J=1→0	CO J=2→1
HPBW	$22''$	$13''$
$\eta_{forward}$	0.90	0.90
η_{beam}	0.60	0.45
Object	NGC 3351	NGC 2903
Date	Oct. 1991	June 1992
Object		NGC 3351
Date		Oct. 1991, June 1992
Object		NGC 3504
Date		June 1992

Table 2. (continued)

Galaxy	Filter	λ_c Å	FWHM Å	t_{exp} sec	seeing $''$
NGC 2903	R			600	1.03
	Hα	6580	40	2x1200	0.92
NGC 3351	R			600	0.79
	Hα	6580	40	2x1200	0.76
NGC 3504	R			600	0.74
	Hα	6600	50	2x1200	0.83

2.2. Optical observations

Broad (R) and narrow band (Hα + [NII]) images of NGC 2903, NGC 3351 and NGC 3504 were obtained at the Cassegrain focus of the 2.5m Nordic telescope located at El Roque de los Muchachos Observatory (Spain). The CCD chip consists of 520 by 520 pixels, each of $0.''196$ projected on the sky, and a field of view of $102'' \times 102''$. A journal of the observational details can be found in Table 2b.

Image reduction and analysis was carried out using the ESO/MIDAS package. Each frame was corrected for bias, non-linearity effects (Kjeldsen 1990), dark current and flat-field in a standard way. The emission line flux and distribution is obtained from the Hα + [NII] filter after subtracting the stellar component. The contribution of the stellar continuum in the narrow-band frames, is obtained applying a two-dimensional isophotal analysis to the R-band, and Hα+[NII] galaxy surface brightness images (see de Juan, Colina, & Golombek 1996). The isophotal analysis is performed over a given range of isophotal radius where no strong emission lines are present. The fraction of stellar light contaminating the emission line flux in the narrow Hα+[NII] filter is calculated as the average of the (Hα+[NII])/R ratio obtained over the selected isophote radius range. The final pure Hα + [NII] emission line image is obtained subtracting the R-band image multiplied by the above calculated average (Hα+[NII])/R factor.

Absolute calibrations of the Hα+[NII] images are obtained using Oke's optical spectrophotometric standards while the Hα fluxes are calculated after correcting for the position of the emission lines in the band-pass and for the contribution of the [NII] lines. To estimate the relative contribution of the [NII]6548,6484Å lines, the Hα and [NII]6584Å equivalent

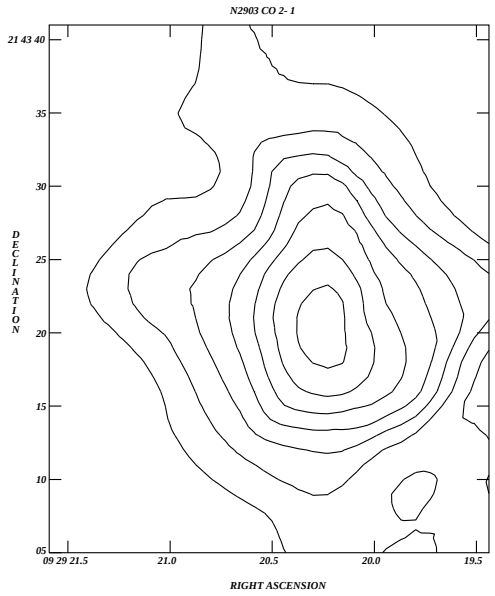

Fig. 1. Distribution of the CO 2→1 integrated emission in NGC 2903. The first contour and the interval are 20 and 10 K km s^{-1}, respectively.

width measurements of Stauffer (1982) have been used. Uncertainties in the central wavelength and shape of the redshift narrow-band filters produce an internal uncertainty of ∼5% in the Hα flux. A correction for internal extinction in the galaxies has not been applied.

3. Circumnuclear molecular gas

The CO J=2→1 emission from the circumnuclear region of the three studied galaxies extends barely over the same area as the Hα emission produced by the burst of star formation (see Sect. 4). Being the nuclear starburst regions a few arcseconds in size, we mapped the molecular gas emission with the highest resolution that can be obtained with a single dish radiotelescope.

3.1. Morphology and kinematics

3.1.1. NGC 2903

The CO J=2→1 spectra obtained toward the central region of this galaxy show an elongated molecular gas distribution along the North-South direction (Fig. 1). The measured (beam convolved) half-intensity size of the CO emission distribution is 21″ × 18″ (approx. NS×EW). This shape and orientation are consistent with the lower angular resolution CO 1→0 map by Jackson et al. (1991), and deviate slightly from the CO 2→1 map by the same authors; such a deviation could be an artifact of the limited number of points observed in the central region by Jackson et al. (1991) and the wider (10″) grid step they used. We obtain a 17″ × 12″ (P.A.=23°) distribution measured at half intensity after deconvolution with a symmetric gaussian beam (HPBW=13″). Although the overall CO distribution is resolved in a 13″ beam, our observations do not show individual peaks, either spatially or kinematically resolved.

The extension and orientation of the observed CO emission is very similar in size and orientation to what is found in mid-infrared (2.2 and 10 μm) and radio continuum wavelengths (Wynn-Williams and Becklin 1985, Ho, Beck & Turner 1989). So, the starburst giving rise to the infrared and radio continuum emission seems to take place over the whole area where CO emission has been detected. The far-infrared emission extends over several minutes of arc, but it retains the overall elliptical shape and a position angle of P.A.∼ 15° (Ghosh et al 1993). Because we are mainly interested in studying the star formation in the inner region of this galaxy, the infrared luminosities quoted in Table 1 do not include the more extended emission. Both L_{IR} and L_{FIR} have been determined from the *IRAS* PSC fluxes exclusively; they correspond to more than half the total luminosities determined from two-dimensional grids by Young et al (1989) and Ghosh et al (1993). Therefore, the infrared luminosities used in our subsequent calculations correspond to an area (∼ 2′ × 2′) larger than that of the measured CO emission (∼ 30″ × 30″), what may lead to an overestimate of the L_{IR}/M_{H_2} and L_{FIR}/M_{H_2} ratios for the circumnuclear region. We consider, however, that this is a reasonable method to estimate those ratios, as no higher resolution infrared observations are available for these galaxies. The use of all the extended infrared emission and all the molecular gas mass detected in a galaxy would give a global value for such ratios that could be very different from the values found in the circumnuclear region. This can be illustrated with observations of NGC 2903. Jackson et al (1991) found L_{FIR}/M_{H_2} = 2.2 $L_\odot$ $M_\odot{}^{-1}$ for the whole galaxy, and $L_{FIR}/M_{H_2} > 7$ $L_\odot$ $M_\odot{}^{-1}$ when the inner 8″ were considered (cf. their §4.3), although they warn that the last ratio could be an order of magnitude larger if the molecular gas in their 21″ beam was distributed over much more than 8″. Our data show that this is what happens, the CO emission distribution being resolved by the 13″ beam. We obtain $L_{FIR}/M_{H_2} \sim 21$ $L_\odot$ $M_\odot{}^{-1}$ for the inner 30″ × 36″, and $L_{FIR}/M_{H_2} > 16$ $L_\odot$ $M_\odot{}^{-1}$ for the inner 8″.

3.1.2. NGC 3351

The profiles taken in the CO 1→0 and 2→1 lines are shown in Figs. 2 and 3, respectively. The integrated intensity CO 2→1 map (Fig. 3) clearly shows that the circumnuclear molecular gas distribution in NGC 3351 has two almost equally bright emission peaks separated by about 11″ (i.e. ∼ 600 pc) with a position angle of ∼ 30°. A two bidimensional Gaussian fit to the total integrated intensity has been performed to determine the previous values. The optical nucleus is not aligned with the CO peaks, and lies 5″ south of the northernmost peak. The orientation and the distance between the two peaks agree completely with the 2.″3 resolution CO 1→0 interferometric map by Kenney et al (1992). In addition to that, our CO 2→1 single-dish map shows extended emission towards the east of the nucleus that is not seen in the interferometer map. This is probably due to the filtering out of the weak, extended emission by the interferometer. Although our two maps agree in the overall aspect, there is a clear difference in the way the southernmost peak appears in the

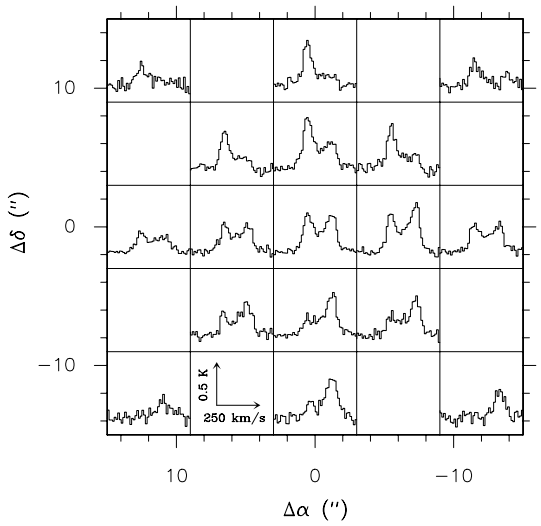

Fig. 2. CO 1→0 emission profiles observed towards NGC 3351, smoothed to a 10.4 km s^{-1} velocity resolution. The velocity and intensity scales are shown at the lower left corner. The velocity range shown in the figure is 500 − 1000 km s^{-1}. The intensity scale corresponds to main beam brightness temperature, as in all other figures showing CO profiles.

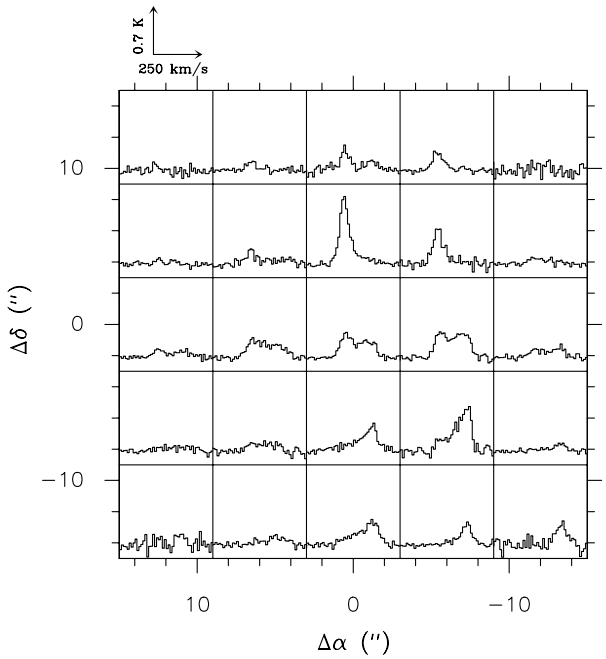

Fig. 3. CO 2→1 emission profiles observed towards NGC 3351, smoothed to a 10.4 km s^{-1} velocity resolution. The velocity and intensity scales are shown at the lower left corner. The velocity range shown in the figure is 500 − 1000 km s^{-1}.

maps.The presence of the two concentrations of molecular gas has been interpreted by Kenney et al (1992) as a consequence of the crowding of gas streamlines near the outer inner Lindblad resonance located ∼ 8″ (400 pc) from the nucleus. This corresponds very well to the observed location of the two CO peaks.

3.1.3. NGC 3504

The molecular gas distribution in this galaxy is more compact than in the previous two galaxies. The sampled area practically covers all the CO emission from this object (Figs. 5 and 6). The individual profiles show the kind of double-peak structure already found in NGC 3351.

The mapped region covers approximately the same area as in Fig. 6 of Kenney, Carlstrom & Young (1993) (hereafter KCY), where a 2.″5 resolution interferometer map of the CO 1→0 emission is shown. The extend of the emission looks different because of the very different angular resolution; in addition to that, the interferometer is quoted to have missed about 30% of the emission, probably the most extended contributions to the flux. Both maps show a monotonically decreasing emission away from the nucleus, with the lowest contour levels oriented SE-NW in both maps. The higher levels, on the other hand, have a rather different position angle (P.A.), ∼ 45° in KCY and ∼ 110° in our single-dish map. The deconvolved size of a gaussian distribution fit to both data is slightly different, 13″ × 7″ in our map as compared to ∼ 5″ in KCY, what can be due to the combined effect of the larger flux we detected and the smearing by the larger beam we used.

Double-peak profiles can be produced by an unresolved rotating ring-like structure, and can also be produced by two concentrations of molecular gas located at the end of a bar, as is the case for NGC 3351. In the case of NGC 3504 the angular resolution of our observations is insufficient to show the presence of a ring or any spatially separated features contributing to the emission. The two CO velocity components seen in the individual profiles are kinematically separated by about 115 km s^{-1}, a velocity difference that is consistent with the two [OIII]5007 velocity components detected within the first 4″ around the nucleus (Heckman et al 1983). Moreover, the CO velocity components are spatially separated by about 5″ along a P.A. of ∼ 120°, as can be determined from a gaussian fit to the emission distribution of each component. Therefore, there are hints that most of the CO emission comes from a ring, or a couple of regions as in NGC 3351, the location of the emission probably being related to the inner inner Lindblad resonance of this galaxy, which is found to be at ∼ 2″ from the nucleus.

The presence of a ring or two emission peaks is not evident in the CO 1→0 channel maps published by KCY (cf. their Fig. 2). A first visual inspection of these maps might suggest that the position of the maximum of emission corresponding to each channel map is located progressively along a line following approximately the stellar bar position angle. A closer inspection shows that there is some crowding of the CO 1→0 emission peaks around three positions. Emission in the range 1459–1524 (5 interferometer channels) is centered on $(\Delta\alpha, \Delta\delta) = (0.''5, -1.''1)$; emission in the range 1550–1602 (4 channels) is centered on

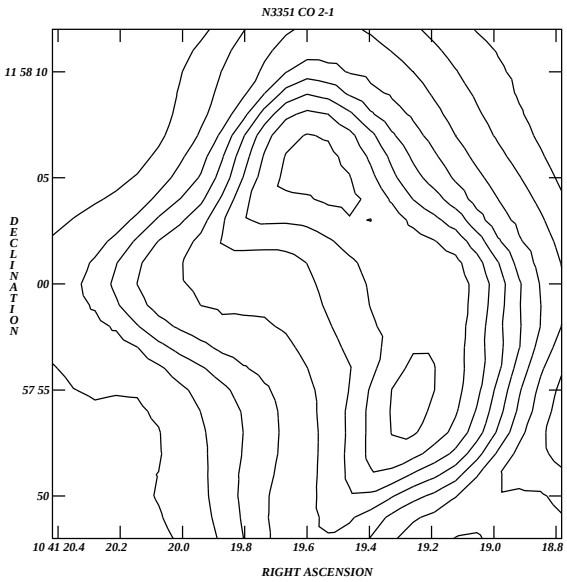

Fig. 4. Distribution of the CO 2→1 integrated emission in NGC 3351. The first contour and the interval are 16 and 8 K km s^{-1}, respectively.

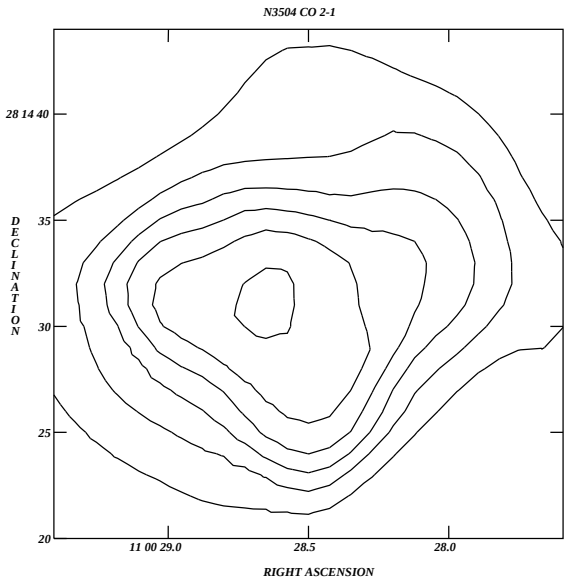

Fig. 6. Distribution of the CO 2→1 integrated emission in NGC 3504. The first contour and the interval are 40 and 20 K km s^{-1}, respectively.

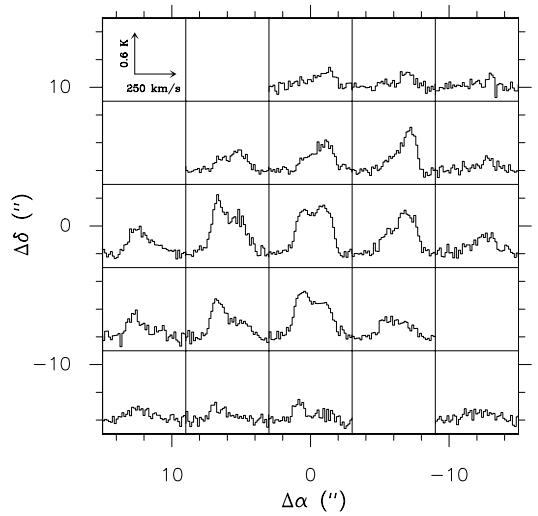

Fig. 5. CO 2→1 emission profiles observed towards NGC 3504, smoothed to a 10.4 km s^{-1} velocity resolution. The velocity and intensity scales are shown at the upper left corner. The velocity range shown in the figure is 1300 − 1800 km s^{-1}.

(−0.″5, 0.″9); and emission in the range 1602–1654 (4 channels) is centered on (−1.″9, 1.″9). The CO 1→0 emission in the lowest velocity range could mostly correspond to the low velocity component found in the CO 2→1 transition, as their centroid velocities practically coincide. The other two velocity components found in the CO 1→0 transition seem to contribute to the high velocity component found in the CO 2→1 transition.

3.2. CO line ratio $R_{21/10}$ for NGC 3351

Our measurements of the two transitions for NGC 3351 allows to estimate the integrated line intensity ratio of the CO lines, after convolving the CO 2→1 map to the angular resolution of the CO 1→0 map. The most significant value (because of a better convolution is achieved) is that of the nucleus and it corresponds to an integrated line ratio (CO 2→1)/(CO 1→0) = 0.8, a value that agrees well with the ones obtained by most authors for isolated galaxies with a normal metallicity (eg, Braine & Combes 1992, Eckart et al 1990, García-Burillo, Guélin & Cernicharo 1993). It is important to realize that, although NGC 3351 is undergoing a starburst, the measured line ratio agrees with the statistical average (Braine & Combes 1992).

This is also the value expected for a giant molecular cloud in our Galaxy. Let us call:

$$R_{21/10} = \frac{\int T_{mb}(\mathrm{CO}\ 2 \rightarrow 1)\mathrm{d}v}{\int T_{mb}(\mathrm{CO}\ 1 \rightarrow 0)\mathrm{d}v}$$

The expected line ratio for an optically thick gas is (e.g. Maloney 1990):

$$R_{21/10} = \frac{11.03/[\exp(11.03/T_{ex}) - 1] - 0.20}{5.52/[\exp(5.52/T_{ex}) - 1] - 0.84}$$

or, to a very good approximation for $T_{ex} > 5$ K, by the much simpler relation

$$R_{21/10} \simeq 1.00 - \frac{2.0}{T_{ex}}.$$

For a typical giant molecular cloud in the Galaxy is T_{ex} = 10 K, then $R_{21/10}$ = 0.80.

3.3. Mass determination and surface density

The existence of an homogeneous line ratio allows us to establish a line intensity to H_2 column density conversion factor for

the CO 2→1 transition and, consequently, to derive the molecular gas mass following an standard procedure applied to the higher angular resolution CO 2→1 measurements. We propose the use of a conversion factor that is 0.8^{-1} times larger that the conversion factor currently used for the CO 1→0 transition, $\chi_{10} = 3.0\ 10^{20}$. Therefore

$$\frac{N(H_2)}{\int T(\mathrm{CO}\ 2 \rightarrow 1)\mathrm{d}v} = \chi_{21} = 3.7\ 10^{20} \quad \mathrm{cm}^{-2}(\mathrm{K\ km\,s}^{-1})^{-1}.$$

that in terms of molecular hydrogen surface density translates into

$$\Sigma_{H_2} = 5.9 \int T(\mathrm{CO}\ 2 \rightarrow 1)\mathrm{d}v \quad \mathrm{M}_\odot\ \mathrm{pc}^{-2}.$$

All the considerations (physical conditions, metallicity) for the use of χ_{10} should apply to χ_{21}.

The results in terms of molecular mass and average surface density for the three observed galaxies can be found in Table 5. The entry *Size* corresponds to the diameter of the area where molecular gas presumably associated to the ionized gas ring and to the starburst is found.

4. Circumnuclear ionized gas

The Hα+[NII] images of starburst galaxies trace the morphology of the circumnuclear ionized gas. This ionized gas is associated to star forming regions of unobscured high surface brightness. In the following sections the major morphological characteristics of the circumnuclear star-forming regions of NGC 2903, NGC 3351 and NGC 3504 are reviewed.

4.1. NGC 2903

The circumnuclear region of this galaxy shows a somewhat irregular morphology as traced by the Hα+[NII] emitting gas (see Fig. 7). The HII regions are spread over an area of $10'' \times 6''$ (or 350 by 210 parsecs) and appear as unresolved or slightly resolved, i.e. with typical sizes $\sim$ 40 parsecs in diameter, or less. The center of the galaxy is considered to be located at the peak of the R band continuum image and is marked by a cross in the Hα+[NII] image (Fig. 7). This assumption seems adequate since the R band peak emission agrees with the peak at 2.2μm (Wynn-Williams & Becklin 1985), which is less affected by dust obscuration.

The line emitting gas distribution in the central $16''$ diameter region is composed of a diffuse component, amounting to 60% of the total emission, and of a few bright compact HII regions amounting to the rest of the flux (Table 3a). Regions R1, R2, R4, and R6 dominate the compact Hα+[NII] emission component (see Fig. 7 and Table 3a).

Although the overall ionized gas distribution agrees well with the radio continuum emission (Wynn-Williams & Becklin 1985), the location of the prominent HII regions do not exactly correspond with the radio continuum emission peaks observed at 2 cm and 20 cm (Wynn-Williams & Becklin 1985; see also Fig. 7). The N and S peaks at 2 cm are displaced by $\sim 1''.5$ with respect to regions R6 and R4, respectively. Moreover, the easternmost 20 cm peak (see Fig. 3a in Wynn-Williams & Becklin 1985) lacks the corresponding optical star-forming counterpart.

The lack of spatial coincidence between the radio continuum and Hα peaks can be understood if the HII regions indicated by the warm Hα emitting gas do not trace the overall star-formation. The radio continuum emission peaks with flat or steep radio spectral indexes could trace regions of massive stars formation in a different evolutionary status (Pérez-Olea & Colina 1995) that are completely obscured at optical wavelengths from our sight. Changes in the morphology of the light distribution at 2.2 μm and 10 μm with respect to V could indicate

Table 3. Circumnuclear HII regions of NGC 2903

Region	Offset $''$, $''$	Diameter* $''$	F(Hα+[NII])$^+$	F(Hα)$^+$
Center		2.0	4.1	3.2
R1	−1.1, +3.7	2.0	14.9	11.4
R2	−2.4, +3.3	2.0	14.9	11.4
R3	−1.6, −0.3	2.0	3.4	2.6
R4	−0.3, −3.3	2.4	13.1	10.1
R5	+1.5, +0.2	2.0	7.5	5.7
R6	+2.3, +2.4	2.4	16.6	12.7
R7	+0.5, +4.0	2.0	9.3	7.2
R8	−0.0, +5.8	2.4	12.0	9.2
Total^{++}		18.0	214.0	164.4

Table 3. (continued)

Region	Offset $''$, $''$	Diameter* $''$	F(Hα+[NII])$^+$	F(Hα)$^+$
Center		2.4	3.6	2.7
R1	+0.4, +6.5	2.4	16.5	12.3
R2	−2.6, +2.6	2.4	21.4	16.0
R3	−1.5, −6.5	2.4	27.7	20.7
R4	+0.5, −5.4	2.2	14.0	10.5
R5	+2.9, −3.5	2.4	6.5	4.9
R6	+4.1, −0.4	2.4	8.2	6.1
R7	+4.8, +3.6	2.2	12.7	9.5
R8	+4.2, +5.6	1.8	3.3	2.5
Total^{++}		18.0	270.0	201.5

Table 3. (continued)

Region	Offset $''$, $''$	Diameter* $''$	F(Hα+[NII])$^+$	F(Hα)$^+$
Center		1.6	9.5	6.0
R1	−2.0, +1.5	1.6	13.8	8.6
R2	−2.0, −0.1	1.6	17.3	10.8
R3	−1.2, −1.5	1.6	16.9	10.6
R4	+0.2, −2.0	1.6	17.7	11.0
Total^{++}		11.0	211.0	131.4

* Diameter of the circular aperture used to measure the flux on each individual HII region. $^+$ in units of 10^{-14} erg s^{-1} cm^{-2} $^{++}$ include the diffuse component

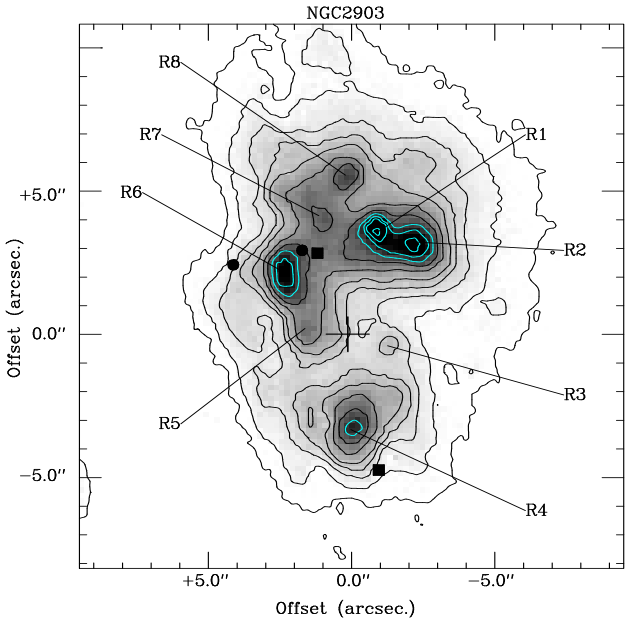

Fig. 7. Hα+[NII] image of NGC 2903, after subtracting the stellar component (see Sect. 2.2 for details). Isophotal contours are overlaid on the gray scale image in order to facilitate the identification of the emission peaks. The observational and the derived characteristics of the bright HII regions can be found in Tables 3a and 4a. The coordinate offsets are referred to the adopted position for the nucleus of the galaxy (see Table 1), the nucleus being indicated by a cross. Black squares and circles indicate the position of the 2 cm and 20 cm radio peaks, respectively.

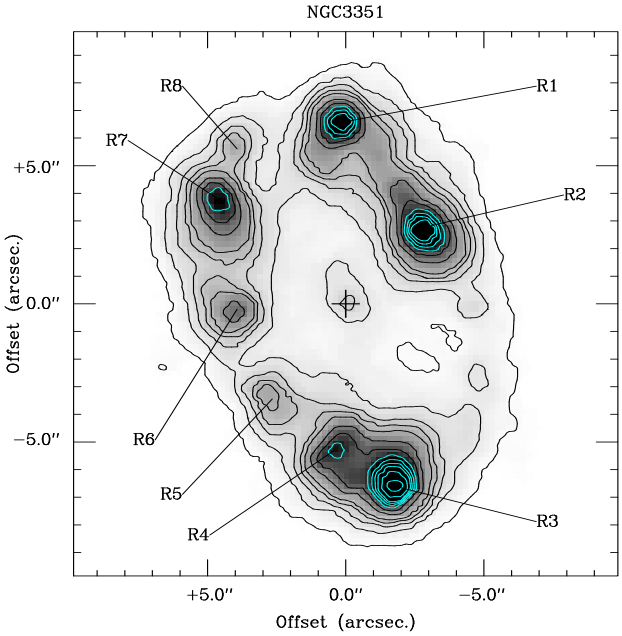

Fig. 8. Hα+[NII] image of NGC 3351, after subtracting the stellar component (see Sect. 2.2 for details). Isophotal contours are overlaid on the gray scale image in order to facilitate the identification of the emission peaks. The observational and the derived characteristics of the bright HII regions can be found in Tables 3b and 4b. The coordinate offsets are referred to the adopted position for the nucleus of the galaxy (see Table 1), the nucleus being indicated by a cross.

the effects of internal obscuration (Wynn-Williams & Becklin 1985).

4.2. NGC 3351

The ionized gas is distributed in a ring-like structure of $13'' \times 6''$, i.e. 0.66 by 0.31 kpc in size, around the nucleus (see Fig. 8). The star forming ring is a complex of several HII regions (labeled R1–R8 in Fig. 8, see also Table 3b) that are unresolved or slightly resolved, i.e. with sizes of $\sim$ 60 parsecs in diameter, or less. This structure is similar, in size and number of individual HII regions detected, to the star-formation ring in NGC 1097 (Hummel, van der Hulst, & Keel 1987).

The position of the nucleus of the galaxy is given by the R-band surface brightness peak, and it is marked with a cross in Fig. 14. The Hα+[NII] emission is dominated by region R3, southwest of the nucleus, and regions R1, R2, and R7 located towards the north of the nucleus. The two peaks of the molecular gas (see Fig. 14 and Kenney et al. 1992) lie very close to regions R1, and R3. There is an elongation of the molecular gas distribution towards region R7, while region R2 seems devoted of a high concentration of molecular gas (see Figs. 4 and 8). As in NGC 2903 and NGC 1097 (Hummel, van der Hulst & Keel 1987), VLA 6 cm observations (Saikia et al. 1994) show the radio continuum emission to be associated to the star-forming ring.

4.3. NGC 3504

The Hα+[NII] image of NGC 3504 (Fig. 9) traces a compact ring structure with a radius of only $2''$ (200 pc) around the nucleus. The ring shows a non closed circular morphology composed of four separated HII regions with an average size of 80 parsecs in diameter, or less. This distribution of HII regions, where the presence of star forming regions is not detected in the NE quadrant can be due to a selective obscuration in the far side of an inclined circumnuclear ring (i = 22°; see Table 1) produced by an excess on the dust and molecular gas surface density towards the NE (see the high resolution CO map in KCY).

The Hα emission is dominated by circumnuclear HII regions, each of them about 1.6 times brighter than the nucleus itself (see Fig. 9 and Table 3c). The ionized and molecular gas share not only a similar spatial distribution but also a similar velocity field. The CO map (Fig. 6) hints the presence of two emission peaks spatially separated by $\sim 4''$ and kinematically separated by 115 km s^{-1}. Evidence for velocity changes by $\sim$ 100 km s^{-1} in the ionized gas across a $4''$ region in the nucleus have been reported by Heckman et al. (1983)

The morphology of the NGC 3504 Hα emitting gas and of the radio continuum emission (Ulvestad, Wilson, & Sramek

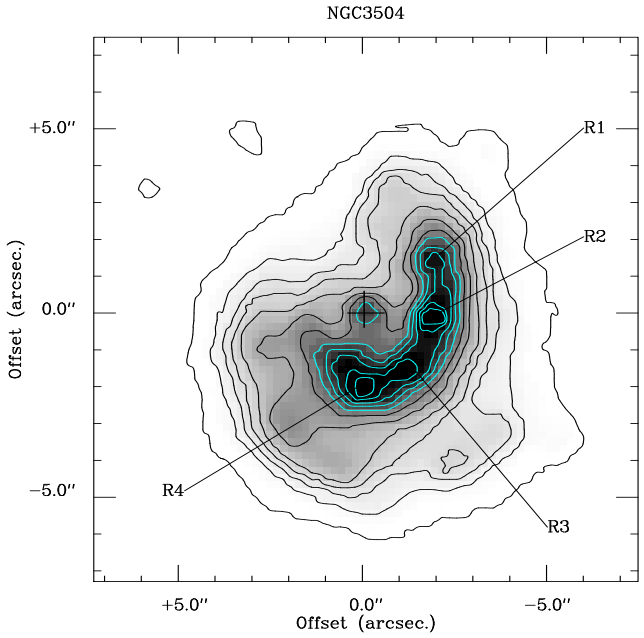

Fig. 9. Hα+[NII] image of NGC 3504, after subtracting the stellar component (see section Sect. 2 for details). Isophotal contours are overlaid on the gray scale image in order to facilitate the identification of the emission peaks. The observational and the derived characteristics of the bright HII regions can be found in Tables 3c and 4c. The coordinate offsets are referred to the adopted position for the nucleus of the galaxy (see Table 1), the nucleus being indicated by a cross.

1981, Saikia et al. 1994) reminds of the compact nucleus plus starburst ring observed in the Seyfert 1 galaxy NGC 7469 (Wilson et al. 1991). A VLA radio map at 2″ resolution shows a central source plus an extended and more diffuse component (Ulvestad, Wilson, & Sramek 1981). The central radio source covers the region occupied by the optical nucleus and the Hα emitting region R1 (Fig. 9), while the extended radio continuum emission agrees in morphology and size with the star-forming ring as traced by the Hα emitting gas.

5. Characterization of the star forming regions

5.1. Ionized gas mass and ionizing flux

The amount of ionized gas associated to each individual star forming region in the circumnuclear regions of the galaxies can be derived from the measured Hα luminosity. For an electron temperature of 10^4 K, one obtains (see e.g. Macchetto et al. 1991)

$$M_g = 3.32\ 10^{-33}\ L(H\alpha)\ N_e^{-1} \quad M_\odot$$

where L(Hα) represents here the Hα luminosity obtained without correction for internal extinction effects. We assume an electron density N_e = 250 cm^{-2} since this is the average electron density measured in the circumnuclear regions of the prototype starburst galaxy NGC 7714 (González-Delgado et al 1995). The results are presented in Tables 4a, 4b & 4c for NGC 2903, NGC 3351, and NGC 3504, respectively. Typical ionized masses for individual HII regions are in the M_g = $10^4 - 10^5$ $M_\odot$ range.

In a similar way, the amount of ionizing photons can be obtained using the Hα luminosity L(Hα) and case B recombination. For an electron temperature of 10^4 K (see e.g Macchetto et al. 1991)

$$N_{ion} = 7.30\ 10^{11}\ L(H\alpha)\ \Omega^{-1} \quad \text{ph s}^{-1}$$

where Ω is the fraction of ionizing photons that is used in the ionization of the surrounding gas. Since a large fraction of the bolometric luminosity of starburst galaxies is radiated at infrared wavelengths as a consequence of dust absorption and reprocessing, a value of Ω= 0.2 is adopted. Values for the ionizing radiation (N_{ion}) in the $10^{51} - 10^{52}$ ph s^{-1} range are measured for individual star-forming regions in these galaxies (see Tables 4a to 4c).

Table 4. Physical properties of the circumnuclear HII regions

(a) NGC 2903

Region	Diam.	L(Hα)	M_g	N_{ion}	SFR
	kpc	10^{38} erg s^{-1}	10^4 M$_\odot$	10^{51} ph s^{-1}	10^{-3} M$_\odot$yr^{-1}
Center	0.07	2.0	0.3	0.7	2
R1	0.07	7.3	1.0	2.7	7
R2	0.07	7.3	1.0	2.7	7
R3	0.07	1.6	0.2	0.6	2
R4	0.08	6.4	0.9	2.4	6
R5	0.07	3.7	0.5	1.3	3
R6	0.08	8.1	1.1	3.0	8
R7	0.07	4.6	0.6	1.7	4
R8	0.08	5.9	0.8	2.2	5
Total	0.63	104.8	13.9	38.3	96

(b) NGC 3351

Region	Diam.	L(Hα)	M_g	N_{ion}	SFR
	kpc	10^{38} erg s^{-1}	10^4 M$_\odot$	10^{51} ph s^{-1}	10^{-3} M$_\odot$yr^{-1}
Center	0.12	3.5	0.5	1.3	3
R1	0.12	15.9	2.1	5.8	15
R2	0.12	20.7	2.8	7.6	19
R3	0.12	26.8	3.6	9.8	25
R4	0.11	13.6	1.8	5.0	13
R5	0.12	6.3	0.8	2.3	6
R6	0.12	8.0	1.1	2.9	7
R7	0.11	12.3	1.6	4.5	11
R8	0.09	3.2	0.4	1.2	3
Total	0.92	260.9	34.7	95.2	240

(c) NGC 3504

Region	Diam.	L(Hα)	M_g	N_{ion}	SFR
	kpc	10^{38} erg s^{-1}	10^4 M$_\odot$	10^{51} ph s^{-1}	10^{-3} M$_\odot$yr^{-1}
Center	0.16	30.4	4.0	11.1	28
R1	0.16	44.0	5.8	16.1	41
R2	0.16	55.2	7.3	20.2	51
R3	0.16	54.2	7.2	19.8	50
R4	0.16	56.6	7.5	20.7	52
Total	1.10	673.8	89.5	245.9	620

The average ionized gas mass and ionizing flux of the individual circumnuclear HII regions in NGC 2903, NGC 3351, and NGC 3504 (Tables 4a-4c) are equivalent to about 100 Orion complexes and correspond to giant HII regions (GEHRs) in external galaxies (Kennicutt 1991). The global ionized gas mass and ionizing power associated to the overall circumnuclear zone in these galaxies are a factor 10 to 20 larger than those measured in individual star forming regions (see Tables 4a to 4c).

One has to bear in mind that the derived values for the amount of ionized mass and ionizing photons, represent a lower limit to these quantities since no correction for internal extinction has been applied. Measurements of the infrared continuum and hydrogen recombination lines for NGC 2903 (Ho, Beck & Turner 1990), NGC 3351 (Puxley, Hawarden & Mountain 1990), and NGC 3504 (Puxley, Hawarden & Mountain 1988) give a mean extinction that is equivalent to a decrease by a factor 3 to 5 in the observed Hα flux emitted by the circumnuclear star forming regions. Thus, on average, the values for the ionized mass and ionizing photons quoted above should be increased by factors three to five, if correction for internal extinction is taken into account.

5.2. Star formation rate

An estimate of the star formation rate (SFR) for each individual star-forming region, as well as for the global circumnuclear star formation can be calculated assuming a star formation process with a constant SFR. Empirical arguments (Doyon, Joseph & Wright 1994) suggest that the star formation in starbursts and luminous IRAS galaxies is biased against the formation of low-mass stars. Based on dynamical mass considerations, Doyon, Joseph & Wright (1994) obtained a value of M_l= 3 $M_\odot$ for the lower mass limit of the initial mass function (IMF). On the other hand, the Brα luminosity measured in a sample of starburst galaxies is best accounted for if the upper mass cut-off lies in the $M_u = 30 - 60$ $M_\odot$ mass range (Ho, Beck & Turner 1990).

Therefore, considering Salpeter's IMF with lower and upper mass limits of M_l = 3 $M_\odot$ and M_u = 60 $M_\odot$, respectively, the SFR is obtained as a function of the Hα luminosity (see e.g. Colina & Pérez-Olea 1992):

$$\mathrm{SFR} = 18.4\ L_{43}(\mathrm{H}\alpha)\ \Omega^{-1} \quad M_\odot\ \mathrm{yr}^{-1}$$

In this expression L_{43}(Hα) indicates the observed Hα luminosity in units of 10^{43} erg s^{-1} while Ω has the same meaning as in Sect. 5.1. For Ω = 0.2 and the previous IMF parameters, a typical SFR between 1.5 10^{-3} $M_\odot$ yr^{-1} and 5.2 10^{-2} $M_\odot$ yr^{-1} for each individual star forming region in these galaxies is obtained. The global star formation rate associated to the circumnuclear zone lies in the 0.1 to 0.6 $M_\odot$ yr^{-1} range (see Tables 4a to 4c).

The above calculated SFR is obtained as a function of the observed Hα luminosity with no correction for internal extinction, and has therefore to be considered as a lower limit. The SFR can also be calculated assuming the same IMF parameters as before but using the infrared luminosity (L_{IR} in Table 1), instead. Following Colina & Pérez-Olea (1992)

$$\mathrm{SFR} = 1.14\ 10^{-10}\ L_{IR}\ \eta^{-1} \quad M_\odot\ \mathrm{yr}^{-1}$$

where L_{IR} is the infrared luminosity in $L_\odot$ and η ($\simeq 1 - \Omega$) gives the fraction of the ionizing and heating luminosity that is absorbed and reprocessed by dust. For η = 0.8, the calculated global star formation rates are factors $\sim$ 3 to 7 larger than the SFR based in Hα luminosity, alone. As already discussed in Sect. 5.1, this discrepancy indicates the effect of internal extinction in deriving parameters for the HII regions based on Hα fluxes. The fact that some of the regions with strongest radio continuum emission do not have an optical counterpart, also indicates the presence of heavily obscured star forming regions (see discussion in Sects. 4.1 and 4.2).

6. Star formation efficiency versus H_2 surface density

6.1. The sample: from normal spirals to luminous IRAS galaxies

The molecular and infrared properties of the starbursts in NGC 2903, NGC 3351, and NGC 3504 plus other galaxies with starbursts associated to a ring of HII regions, and for which CO maps of similar angular resolution are available, are summarized in Table 5. Hereafter we will refer to these galaxies as circumnuclear starburst galaxies. In this table, *size* refers to the region where molecular gas presumably associated to the ionized gas ring and, therefore, to the circumnuclear starburst is found. The quoted sizes are not corrected for the beam size. It can be argued that in some cases (like NGC 3504) the optical ring is considerably smaller that the quoted size and that could change the relevant parameters, Σ_{H_2} and $L_{\mathrm{IR}}/M_{\mathrm{H_2}}$. In the case of NGC 3504, if we consider the mass detected by us in one beam (76% of the mass quoted in Table 5) or by KCY with an interferometer (71% of their own single-dish mass) and we take the fraction of the infrared luminosity associated to the starburst (i.e., excluding that of the disk), which is 59% of the total luminosity according to Rowan-Robinson & Crawford (1989), the $L_{\mathrm{IR}}/M_{\mathrm{H_2}}$ would be 10 $L_\odot$ $M_\odot{}^{-1}$, not significantly lower than the value quoted in Table 5.

Also, an homogeneous set of data have been gathered from the literature to compare the IR luminosity and molecular gas content of circumnuclear starburst galaxies against normal spirals, Seyferts with starbursts, and luminous IRAS galaxies. The information for IRAS galaxies is shown in Table 6, which also includes data for two nearby, well studied galaxies (M33, M51), and values corresponding to the inner part of the Milky Way including the molecular gas ring. The median values found by Scoville and Good (1989) for giant molecular clouds in the Milky Way associated to giant HII regions (GMC w/ HII) and giant molecular clouds without HII regions (GMC w/o HII) are also indicated. (See footnotes in Table 6 for specific references.)

Distances for the starburst sample are calculated from the 21cm heliocentric velocity when available (de Vaucouleurs et al. 1991). For the rest of the starburst galaxies and for the IRAS galaxies, distances are calculated from the heliocentric velocity obtained from the optical or CO emission lines. A Hubble constant $H_\circ$ = 75 km s^{-1}Mpc^{-1} is considered throughout. When in the original reference a different distance is used, total molecular hydrogen mass $M_{\mathrm{H_2}}$, and size are scaled to the new distances

Table 5. H_2 and IR properties of circumnuclear starburst galaxies

Galaxy	Type	Distance	Size	L_{IR}	M_{H_2}	Σ_{H_2}	L_{IR}/M_{H_2}	Ref
		Mpc	kpc	10^9 $L_\odot$	10^8 $M_\odot$	$M_\odot$ pc^{-2}	$L_\odot$ $M_\odot^{-1}$	
NGC 1068	Sy2	15.1	3.2	217.7	52	740	42	1
NGC 1068$^+$	AGN	15.1	0.21	109.0	0.8	2300	1360	2
NGC 1068^{++}	starburst	15.1	2.0-3.2	109.0	> 25	> 510	< 44	2
NGC 1097	Liner/Sy1	17.0	1.6	42.1	12	600	35	3
NGC 2903	starburst	7.3	1.0	6.0	1.8	240	33	this work
NGC 3227*	Sy1	15.1	0.6	7.2	5.8	2000	12	4
NGC 3351	starburst	10.4	1.4	6.0	3.5	230	17	this work
NGC 3504	Liner/starburst	20.7	2.7	28.1	21	370	13	this work
NGC 4321	starburst	21.1	2.2	30.8	16.3	430	19	4
NGC 7469	Sy1	65.5	2.0	366.	74	> 2400	50	5

$^+$ IR luminosity emitted by the AGN and H_2 mass around the nucleus.
$^{++}$ IR luminosity emitted by the starburst ring and H_2 mass associated to the starburst ring.
* Recent Hα images by González-Delgado (1995) show a partial ring of HII regions at the distance of the inner Lindblad resonance radius.
References: (1) Planesas, Gómez-González, & Martín-Pintado 1989; (2) Planesas, Scoville, & Myers 1991; (3) Gerin, Nakai, & Combes 1988; (4) Braine et al. 1993; (5) Sanders et al. 1988.

Table 6. H_2 and IR properties for IRAS galaxies, spirals and giant molecular clouds

Galaxy	Distance	Diameter	L_{IR}	M_{H_2}	Σ_{H_2}	L_{IR}/M_{H_2}	Ref
	Mpc	kpc	10^{11} $L_\odot$	10^9 $M_\odot$	$M_\odot$ pc^{-2}	$L_\odot$ $M_\odot^{-1}$	
VII Zw31	221	$<$7.6	8.6	41.4	$>$910	21	1
IRAS10173+0828	197	$<$6.9	5.3	9.0	$>$240	59	2
IRAS17208$-$0014	175	3.4	21.9	55.0	6100	40	2
Mrk 231	174	$<$6	31.9	32.4	$>$1200	100	1
Arp 55	163	6.4	4.8	26.5	820	18	3
NGC 6240	101	3.4	6.5	15.1	1700	43	4
VV 114	78	3.0	3.9	14.7	2100	27	1
Arp 220	77	0.5 x 0.7	14.6	18.3	66000	80	5
NGC 828	72	1.8	2.1	18.4	7200	11	3
NGC 1614	62	1.2	3.8	4.6	4100	83	1
Zw 049.057	52	0.9	1.5	3.9	6100	38	2
IC 694	42	$<$0.5	3.3	3.9	$>$20000	85	6
NGC 520	29	0.8	0.7	3.3	6600	21	3
NGC 4038	21	0.8	0.5	0.8	1600	63	7
NGC 3079	15	0.4 x 1.0	0.3	2.4	7600	13	8
NGC 2146	11	0.4 x 1.4	0.5	1.8	4100	28	9
M 51	9.6	2.3	0.11*	0.8	200	14	10, 11
M 33	0.8	1.6	0.001	0.034	17	2.9	12, 13
Milky Way		14	0.08	2	13	4	14, 15
GMC w/ HII		0.069	$2\ 10^{-5}$	$6\ 10^{-4}$	130	7	16
GMC w/o HII		0.021	$3\ 10^{-7}$	$8\ 10^{-5}$	110	1	16

* Luminosity calculated multiplying by 1.9 the IR luminosity in reference (11) to transform to the $8-1000\mu$m luminosity.
References: (1) Scoville et al. 1989; (2) Planesas, Mirabel, & Sanders 1991; (3) Sanders et al. 1988; (4) Wang, Scoville, & Sanders 1991; (5) Scoville et al. 1991; (6) Sargent & Scoville 1991; (7) Stanford et al. 1990; (8) Young, Clausen & Scoville 1988; (9) Young et al. 1988; (10) García-Burillo, Guélin, & Cernicharo 1993; (11) Smith 1982; (12) Wilson & Scoville 1989; (13) Rice et al. 1990; (14) Solomon et al. 1987; (15) Scoville & Soifer 1991; (16) Scoville & Good 1989.

(as listed in Table 5 and 6). For IRAS galaxies, *Diameter* refers to the measured size of the molecular gas distribution. In some cases this size is heavily dominated by the beam size and no deconvolution has been applied. When the source is completely unresolved the beam size (in kpc) is quoted as an upper limit for the molecular gas distribution diameter.

The column labeled L_{IR} in Tables 5 and 6 refers to the total luminosity in the 8-1000 μm range and it is calculated using the fluxes in the four IRAS bands according to Perault (1987). This infrared luminosity gives about twice the value of L_{FIR}, luminosity in the range 40-120 μm, as obtained from the 60 and 100 μm IRAS fluxes (Fullmer & Lonsdale 1989).

The column labeled M_{H_2} in Tables 5 and 6 represents the mass of molecular gas rescaled, when necessary, to the conversion factor used in this paper, $\chi_{10} = 3\ 10^{20}$ cm^{-2} (K km s^{-1})$^{-1}$. Molecular gas in the selected IRAS galaxies has been observed with millimeter-wavelength interferometers, so the mass of the molecular gas measured in these galaxies comes from regions with a linear size similar to that of nearby circumnuclear starburst galaxies. For the IRAS galaxies, no correction is applied for missing flux from a more extended component.

It can be argued that the use of the χ_{10} conversion factor overestimates the total gas mass, as the gas temperature in the sample of galaxies is probably higher than in molecular clouds in the Milky Way. In fact, the average gas temperature is 10 K, and the average 60/100 color dust temperature is 29 K for GMCs in the Milky Way disk (Scoville and Good, 1989), while the dust temperature for the IRAS galaxies in the sample is in the range 35-50 K. If a higher dust temperature indicates a higher excitation gas temperature, the conversion factor would be overestimated in these objects, as it depends on density n_{H_2} and temperature T according to $\chi_{10} \propto \sqrt{n_{H_2}}/T$ (Dickman, Snell & Schloerb 1986). However, their high H_2 surface density, often an order of magnitude larger than for a GMC in the Milky Way, tells us that either the filling factor of molecular clouds is close to 1, or that the average density of a GMC in IRAS galaxies is higher than in a normal galaxy, or that both causes contribute to the measured high H_2 surface density. The decrease in the χ_{10} conversion factor due to a higher gas temperature could be compensated in part by an increase in the average gas density. As a conclusion, a decrease of the total M_{H_2} by a factor larger than two due to the different physical conditions seems unlikely.

The column labeled Σ_{H_2} refers to the H_2 surface density obtained considering the H_2 mass is uniformly distributed in the circular area given by the quoted diameter. The quoted values for Σ_{H_2} have to be considered lower limits in the IRAS galaxies, mainly because of the size assumed for the gas distribution, in excess due to the insufficient angular resolution of the observations. In addition to that, the interferometer may have missed part of the flux that would contribute to the gas mass. Even if the total mass is decreased as explained in the previous paragraph, values for Σ_{H_2} in IRAS galaxies may be higher than the ones quoted in Table 6.

The star formation efficiency (SFE) is measured, as usual, as the infrared luminosity per unit of molecular gas mass, L_{IR}/M_{H_2}. Fig. 16 shows the L_{IR}/M_{H_2} ratio versus the H_2 surface density (Σ_{H_2}) for the inner regions of the galaxies in Table 5, the luminous IRAS galaxies in Table 6, the galaxies M33, M51, and the Milky Way, and for the "median" of two populations of GMCs in the Milky Way. The distribution of Σ_{H_2} extends over four orders of magnitude if normal, non-starburst spiral galaxies are included, for which $\Sigma_{H_2} \sim 10^1$ M$_\odot$pc^{-2}, and reaches values in excess of 10^4 M$_\odot$pc^{-2} for ultraluminous IRAS galaxies with huge concentrations of molecular gas near the nucleus. The distribution of L_{IR}/M_{H_2} extends only over two orders of magnitude, being $\sim 10^0$ L$_\odot$ M$_\odot{}^{-1}$ for galactic GMCs w/o HII, $< 10^1$ L$_\odot$ M$_\odot{}^{-1}$ for GMCs w/ HII, the Milky Way and M33, and between 10^1 L$_\odot$ M$_\odot{}^{-1}$ $< L_{IR}/M_{H_2} <$ 10^2 L$_\odot$ M$_\odot{}^{-1}$ for circumnuclear starbursts, Seyferts, and luminous IRAS galaxies. We caution that all values for these galaxies refer to the circumnuclear regions indicated by the quoted size or diameter.

In what follows, the distribution of star formation efficiencies, of molecular gas surface densities, and the relative distribution of both of them will be discussed. All the discussion below refers to the values presented in Tables 5 and 6 and shown in Fig. 16.

6.2. Circumnuclear starburst galaxies

The sample consists of eight galaxies of which NGC 1068, NGC 1097, NGC 3227, NGC 3504 and NGC 7469, are a combination of starburst ring and active galactic nucleus (SB+AGN hereafter). The rest of the sample (NGC 2903, NGC 3351 and NGC 4321) are pure starburst or nuclear-starburst galaxies (SB hereafter).

This sample covers the range of $10^2 - 10^3$ M$_\odot$ pc^{-2} in molecular gas surface density and the range of $10 - 50$ L$_\odot$ M$_\odot{}^{-1}$ in star formation efficiency. If the infrared luminosity in the starburst galaxies is dominated by the energy output directly associated to the circumnuclear starburst, the global SFR can be computed considering the same IMF parameters as in Sect. 5.2. The resulting SFR values are in the range $1 \leq$ SFR ≤ 40 M$_\odot$ yr^{-1} with an average value of SFR ~ 5 M$_\odot$ yr^{-1}.

The SFE expected from a starburst can be modeled and compared with the empirical results. Assuming Salpeter's initial mass function (IMF) with mass limits $M_l = 3$ M$_\odot$ and $M_u =$ 60 M$_\odot$ (see Sect. 5.2), and a constant star formation rate over the last τ_{SF} years, the expected star formation efficiency of the starburst as given by $L_{IR}^{SB}\ [M_{H_2}^{SB}]^{-1}$ is

$$L_{IR}^{SB}\ [M_{H_2}^{SB}]^{-1} = 8.74\ 10^9\ \eta\ \epsilon^{SB}\ \tau_{SF}^{-1} \quad L_\odot\ M_\odot^{-1}$$

where ϵ^{SB} is given by

$$\epsilon^{SB} = \text{SFR}\ \tau_{SF}[M_{H_2}^{SB}]^{-1}$$

In this expression, ϵ^{SB} represents the fraction of molecular gas that can be converted into stars over the starburst phase, if a steady-state in the star formation rate is considered. The star formation rate (SFR) and L_{IR}^{SB} are obtained following Colina & Pérez-Olea (1992). Therefore, the $L_{IR}^{SB}\ [M_{H_2}^{SB}]^{-1}$ ratio can be calculated if the duration of the star formation process (τ_{SF}) is assumed.

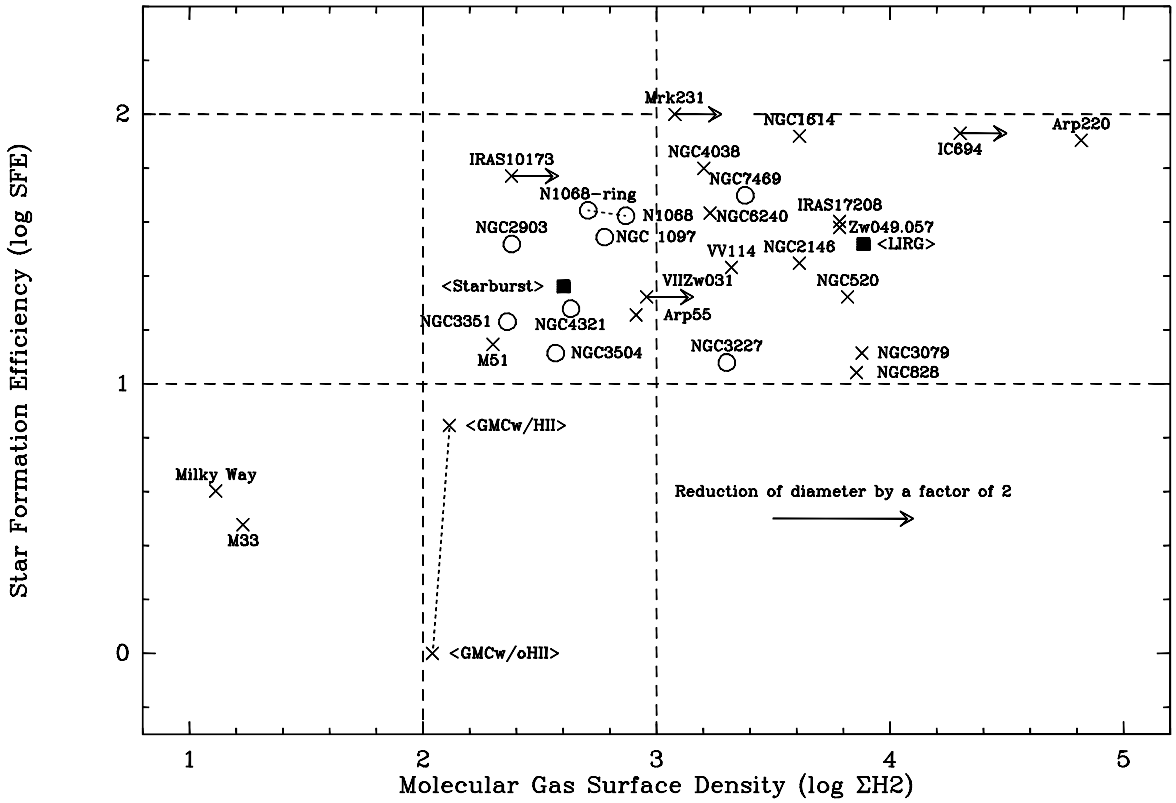

Fig. 10. Plot of the observed star formation efficiency, as measured by the $L_{\rm IR}/M_{\rm H_2}$ ratio, vs. the molecular gas surface density, Σ_{H_2}, for circumnuclear starburst galaxies (open circles, see Table 5), luminous IRAS galaxies (Table 6), the galaxies M33, M51, and the Milky Way, and for the "median" of two populations of GMCs in the Milky Way, those with and without associated HII regions. Lower limits to the Σ_{H_2} are plotted for some galaxies, because the molecular gas emission has not been resolved due to insufficient angular resolution in the observations. The change in Σ_{H_2} produced by a reduction of the assumed diameter by a factor of two is indicated by the length of an arrow in the lower right corner. The data point labeled `N1068-ring` corresponds to the molecular ring of the prototype Seyfert 2 galaxy NGC 1068. The overall CO emission up to a radius of 1.6 kpc (including the ring) is represented in `NGC1068`. Data points corresponding to average values are indicated by black squares. < `starburst` > indicates the average of the circumnuclear starburst galaxies in Table 5, excluding those galaxies that host an AGN. < `LIRG` > indicates the average value for the luminous IR galaxies in Sanders, Scoville and Soifer (1991).

Arguments based on the energy release expected in a starburst will be used to estimate τ_{SF}. The overall kinetic energy generated in massive star formation processes over a few 10^7 years is due to supernova explosions and mass-loss winds in massive stars, and corresponds to $\sim 10^{57}$ erg s^{-1} (Colina, Lipari & Macchetto 1991). This energy is able to move large amounts of gas ($10^9 - 10^{10}$ M$_\odot$) to velocities larger than the internal dispersion velocity measured in individual giant molecular clouds ($\sim$ 10 km s^{-1}, eg. Scoville et al 1987), destroying therefore the molecular clouds where star formation is taking place (see also Sect. 6.4). Therefore, for η= 0.8 and a typical duration of the starburst of $\tau_{\rm SF} \leq 3\ 10^7$ yr, $L_{\rm IR}^{\rm SB}\ [M_{\rm H_2}^{\rm SB}]^{-1} \geq 233\ \epsilon^{\rm SB}$.

A value $\epsilon^{\rm SB} \leq 0.10$ is obtained comparing the calculated $L_{\rm IR}^{\rm SB}\ [M_{\rm H_2}^{\rm SB}]^{-1}$ with the mean, $<L_{\rm IR}^{\rm SB}\ [M_{\rm H_2}^{\rm SB}]^{-1}>$ = 23 L$_\odot$ M$_\odot{}^{-1}$, of the values measured in circumnuclear starburst galaxies: NGC 1068 starburst ring, NGC 2903, NGC 3351, NGC 3504, and NGC 4321. This large value for $\epsilon^{\rm SB}$ indicates an overall high efficiency in the gas to stars conversion in the circumnuclear molecular clouds, over the whole period of the starburst (see Sect. 6.4). The value of $\epsilon^{\rm SB}$ around 0.10 would also imply that most of the dynamical mass in the circumnuclear star forming regions is still in the form of molecular gas. There is some observational evidence supporting this conclusion; in most of the luminous IRAS galaxies the molecular mass around the nucleus is very close to the value of the dynamical mass (Scoville et al. 1991).

In the $L_{\rm IR}/M_{\rm H_2} - \Sigma_{\rm H_2}$ diagram (Fig. 16), circumnuclear starburst galaxies are well separated from normal spiral galaxies like the Milky Way and M33. The lower limit for the $\Sigma_{\rm H_2}$ in circumnuclear starburst galaxies is similar to the $\Sigma_{\rm H_2}$ for GMCs in the Milky Way. Therefore, if most of the H_2 mass in starburst galaxies is in GMCs, then their overall surface filling factor in the region where the starburst occurs would be very high.

The lower values of the $L_{\rm IR}/M_{\rm H_2}$ for circumnuclear starburst galaxies and IRAS galaxies is $\sim$ 10 L$_\odot$ M$_\odot{}^{-1}$, close to the median for the GMC w/ HII (see Table 6), what could indicate that the molecular gas is predominantly found in molecular clouds where star formation takes place. However, the fact that

the average $L_{\rm IR}/M_{\rm H_2}$ for starbursts is a factor three higher than for GMC w/ HII, can be interpreted as an increase by the same factor in the gas to stars conversion ($\epsilon^{\rm SB}$) of molecular clouds in starburst galaxies with respect to GMC w/ HII, if the same mass limits on the initial mass function and time duration $\tau_{\rm SF}$ are considered.

On the other hand, if the star formation in GMC w/ HII and in circumnuclear starburst galaxies have a different lower mass limit, i.e., IMF in the Milky Way GMC w/ HII has a lower mass limit of 0.1 $M_\odot$ as compared to the 3 $M_\odot$ for starbursts, the corresponding $L_{\rm IR}/M_{\rm H_2}$ will be given by

$$(L_{\rm IR}/M_{\rm H_2})^{\rm GMCw/HII} = 1.93\ 10^9\ \eta\epsilon^{\rm GMCw/HII}\tau_{\rm SF}^{-1} \quad L_\odot\ M_\odot{}^{-1}$$

The observed $L_{\rm IR}^{\rm SB}\ [M_{\rm H_2}^{\rm SB}]^{-1}/(L_{\rm IR}/M_{\rm H_2})^{\rm GMCw/HII}$ ratio of ~ 3 would then translate into a relative decrease by a factor of ~ 0.7 in the gas to stars conversion in the circumnuclear molecular clouds with respect to GMC w/ HII, provided the same $\tau_{\rm SF}$ is considered.

There are some nearby starburst galaxies that also harbor an AGN-type source. NGC 1068 is the only case in which separate values for the $L_{\rm IR}/M_{\rm H_2}$ ratio associated to the AGN, to the starburst (SB) ring, and to the combined SB+AGN can be calculated empirically. Half of the total infrared emission is assumed to come from the nucleus and the other half from the starburst ring (Telesco et al 1984). The total molecular mass in the inner 1.6 kpc radius is 5.2 10^9 $M_\odot$ as determined from single-dish observations (Planesas et al. 1989). A lower limit of 2.5 10^9 $M_\odot$ to the molecular gas mass in the starburst ring is given by the CO flux detected by interferometer observations (Planesas, Scoville & Myers 1991). These observations may have missed the more diffuse component of the molecular gas associated to the starburst ring, explaining therefore the factor of 2 discrepancy in the molecular mass measured by interferometer and single-dish observations. The interferometer observations also revealed the presence of $\sim 8\ 10^7$ $M_\odot$ of molecular gas toward the nucleus, distributed in a region not resolved by the 2.″9 beam (Planesas, Scoville and Myers 1991).

The infrared luminosity and molecular gas associated to the AGN in the nucleus of NGC 1068 (see Table 5), give an infrared luminosity to molecular mass ratio equivalent to $(L_{\rm IR}/M_{\rm H_2})^{\rm AGN} = 1360\ L_\odot\ M_\odot{}^{-1}$. On the other hand, for the star-forming ring $21\ L_\odot\ M_\odot{}^{-1} < L_{\rm IR}^{\rm SB}\ [M_{\rm H_2}^{\rm SB}]^{-1} < 44\ L_\odot\ M_\odot{}^{-1}$, depending on whether the single-dish or the interferometer measurements are considered. The $L_{\rm IR}/M_{\rm H_2}$ ratio calculated for the starburst ring is similar to the overall AGN plus starburst, $(L_{\rm IR}/M_{\rm H_2})^{\rm SB+AGN} = 42\ L_\odot\ M_\odot{}^{-1}$ (Table 5). This is easily understood because the AGN infrared luminosity equals that of the star-forming ring but the molecular gas in the first ~ 100 pc around the nucleus amounts to less than 3% of the molecular gas associated to the starburst ring (see Table 5).

In galaxies like NGC 1068 showing evidence of an AGN and a circumnuclear starburst (SB+AGN), the observed SFE can be understood in first order considering that the AGN infrared luminosity is a factor α of the starburst infrared luminosity ($L_{\rm IR}^{\rm SB}$), and that the global molecular gas mass corresponds to the molecular gas mass associated to the starburst ($M_{\rm H_2}^{\rm SB}$). Therefore, the $L_{\rm IR}/M_{\rm H_2}$ ratio is given by

$$(L_{\rm IR}/M_{\rm H_2})^{\rm SB+AGN} \approx\ (1+\alpha)\ L_{\rm IR}^{\rm SB}\ [M_{\rm H_2}^{\rm SB}]^{-1}$$

where $\alpha \approx 1$ for NGC 1068, as half of the infrared luminosity comes from the active nucleus (see Table 5). The SB+AGN scenario presented for NGC 1068 could also be valid for the rest of the galaxies in the SB+AGN and for the luminous IRAS galaxies (see Sect. 6.3). Some Seyfert 1 galaxies like NGC 7469, with known star-forming rings, would represent the case where the AGN infrared luminosity contribution would be about 50% ($\alpha \sim 1$) of the total (Table 5), if the average $<L_{\rm IR}^{\rm SB}\ [M_{\rm H_2}^{\rm SB}]^{-1}> = 23\ L_\odot\ M_\odot{}^{-1}$ for pure starbursts is considered.

6.3. Nearby circumnuclear starburst galaxies versus luminous IRAS galaxies

IRAS galaxies tend to have a H_2 surface density higher than circumnuclear starburst galaxies. The latter are found in the range $10^2\ M_\odot\ pc^{-2} < \Sigma_{H_2} < 10^3\ M_\odot\ pc^{-2}$, while IRAS galaxies have $\Sigma_{H_2} > 10^3\ M_\odot\ pc^{-2}$. An upper limit is not well established because the lack of angular resolution does not allow to deconvolve the measured distribution of molecular gas; this limit could well be in excess of $10^5\ M_\odot\ pc^{-2}$

All galaxies undergoing a starburst (including the IRAS galaxies) have $10^1\ L_\odot\ M_\odot{}^{-1} < L_{\rm IR}/M_{\rm H_2} \leq 10^2\ L_\odot\ M_\odot{}^{-1}$. Also, for a given value of Σ_{H_2}, the values of the $L_{\rm IR}/M_{\rm H_2}$ ratio are spread over one order of magnitude. No trend for $L_{\rm IR}/M_{\rm H_2}$ to increase with Σ_{H_2} is apparent from this data, in disagreement with what has been found by other authors (Scoville et al. 1991). The upper limit for the $L_{\rm IR}/M_{\rm H_2}$ ratio appears well defined, as it extends over at least three orders of magnitude in gas surface density, Σ_{H_2}. This upper limit is $L_{\rm IR}/M_{\rm H_2} \sim 10^2\ L_\odot\ M_\odot{}^{-1}$, although it could be twice larger if the uncertainties in χ_{10} are taken into account (see Sect. 6.1). It is also clear that the existence of such an empirical upper limit for the $L_{\rm IR}/M_{\rm H_2}$ ratio is independent of the Σ_{H_2} and of the M_{H_2} found in the inner regions of all these galaxies.

The population of galaxies with an AGN do not show any peculiar distribution in the $L_{\rm IR}/M_{\rm H_2}$ vs. Σ_{H_2} plot, some of the AGN galaxies being found close to the $L_{\rm IR}/M_{\rm H_2}$ upper limit (eg, the Sy1 ultraluminous infrared galaxy Mrk 231), others close to the lower limit (eg, the Sy1 NGC 3227). We conclude that the presence or absence of an AGN in a starburst galaxy does not change drastically its SFE. However, the value of the SFE as measured from $L_{\rm IR}/M_{\rm H_2}$ is an overestimate of the $L_{\rm IR}^{\rm SB}\ [M_{\rm H_2}^{\rm SB}]^{-1}$ when the contribution of the AGN to the $L_{\rm IR}$ is important.

In fact, star formation alone has difficulties in explaining a large observed $L_{\rm IR}/M_{\rm H_2} \sim 100\ L_\odot\ M_\odot{}^{-1}$ limit. $L_{\rm IR}/M_{\rm H_2}$ indicates the amount of luminosity per unit of mass. For stars, the L/M ratio goes as proportional to $M^{2.8}$. Therefore only stars with masses above $5M_\odot$ have a L/M ratio above 100. In a star formation process, the total mass in stars is dominated by the less massive stars, 1-2 $M_\odot$ or less. Since the mass in molecular gas is the major contributor to the total dynamical mass in starbursts environments, it can be concluded that only if the

initial mass function (IMF) were restricted to stars with masses $M_{star} \geq 10\ M_\odot$, could a L_{IR}/M_{H_2} ratio of the order of 100 $L_\odot\ {M_\odot}^{-1}$, or larger, be obtained. Considering that the average $<L_{IR}^{SB}\ [M_{H_2}^{SB}]^{-1}>$ in nearby starburst galaxies is 23 $L_\odot\ {M_\odot}^{-1}$ (Sect. 6.2), it seems very unlikely that a different IMF biased towards an even higher lower mass limit could exist in luminous IRAS galaxies, in general.

There is however an alternative to explain the L_{IR}/M_{H_2} range and upper limit observed in luminous IRAS galaxies. Many of the luminous IRAS galaxies in Table 6 show the optical characteristics associated to Seyfert 2 galaxies or LINERs. Therefore, if luminous IRAS galaxies are versions of NGC 1068 at larger distances, the range in the L_{IR}/M_{H_2} ratio and its upper limit can be understood as a consequence of an increase in the AGN contribution to the global infrared luminosity (the α parameter in the previous equation).

Considering that the mean SFE associated to a circumnuclear starburst is $<L_{IR}^{SB}\ [M_{H_2}^{SB}]^{-1}>= 23\ L_\odot\ {M_\odot}^{-1}$, the observed range in the L_{IR}/M_{H_2} ratio of luminous IRAS galaxies translates into $0 \leq \alpha \leq 3$, i.e., the infrared luminosity from the AGN corresponds to a $\sim 10\% - 75\%$ of the total IR luminosity measured in these galaxies. This is also the case for the UV-excess quasar Mrk 1014 where a L_{IR}/M_{H_2} of 43 $L_\odot\ {M_\odot}^{-1}$ (i.e., α = 1) has been measured (Sanders, Scoville, & Soifer 1988). A similar conclusion, i.e., that many radio-quiet active galaxies have powerful circumnuclear starbursts, is obtained from the FIR−radio luminosity correlation observed in starburst galaxies, Seyferts, luminous IRAS galaxies, and QSOs (Colina & Pérez-Olea 1995).

6.4. Overall physical scenario

The basic empirical results that can simultaneously fit all the characteristics of the observed $L_{IR}/M_{H_2}-\Sigma_{H_2}$ relation in nearby starbursts, Seyferts with starbursts, and luminous IRAS galaxies can be summarized in three main conclusions: (i) molecular clouds in the nuclear/circumnuclear regions have associated HII regions, (2i) the total gas into stars conversion in these molecular clouds is about 10% or less, i.e., $\epsilon^{SB} \leq 0.10$, if the star formation processes are short lived (3 10^7 years) and biased towards a high lower limit of the IMF ($M_l \sim 3\ M_\odot$), and (3i) the presence of an additional AGN energy source can explain extreme cases for which the L_{IR}/M_{H_2} is close to 100 $L_\odot\ {M_\odot}^{-1}$.

How could all these properties fit into a more general physical picture? Our results are discussed in the context of the gravitational instability model of star formation by Elmegreen (1994). Under the gravitational instability model (GIM hereafter), the critical parameter to induce a large star formation process in the nuclei or circumnuclear regions of galaxies is the extremely high value of the gas density. Under this scenario, the starburst has three phases:

(1) The *accretion phase* when the gas accretes to the center of the galaxy, or in a ring around the inner Lindblad resonance (ILR hereafter). This situation is obvious in many nearby starbursts like NGC 1068 (Planesas, Scoville & Myers 1991), NGC 3351 (Devereux, Kenney & Young 1992), and NGC 3504 (KCY) where a molecular ring associated with the ILR has been detected. Also, merger processes involving two large spiral galaxies induce large concentrations of molecular gas in the nuclear regions of luminous IRAS galaxies.

(2) The *turn-on phase* when the density reaches a high critical value. While average densities in the outer galactic regions are low, 1–10 cm^{-3}, molecular gas densities averaged over the entire volume of the molecular gas region in nearby starbursts are $> 10\ cm^{-3}$ with the lower limit larger than $> 2\ 10^2\ cm^{-3}$ in some individual molecular clumps like those observed in the molecular ring of NGC 1068 (Planesas, Scoville & Myers 1991). For luminous IRAS galaxies, average gas densities are even larger with cases as extreme as Arp220 where densities in excess of $3\ 10^3\ cm^{-3}$ are inferred (cf. Table 6).

(3) The *starburst phase* when the star formation proceeds in a high density environment at a extremely high rate. It is clear from Fig. 13−15 that the galaxies NGC 2903, NGC 3351, and NGC 3504 are in an active phase of generating young massive stars at an average rate of SFR $\sim 2\ M_\odot\ yr^{-1}$, if M_l = 3 $M_\odot$. Similar conclusions are obtained for starbursts and luminous IRAS galaxies when estimating the star formation rates using recombination lines or the infrared luminosity.

Once the starburst starts, the GIM is able to predict the properties of the star formation process like the duration, rate, and efficiency of the star formation, and the mass limits of the initial mass function (IMF). Under the GIM, the duration of the star formation (τ_{SF}) and the star formation rate (SFR) depend on the gas density with $\tau_{SF} \propto \rho^{-0.5}$ and SFR $\propto \rho^{1.5}$, respectively (Elmegreen 1994). Consequently, since densities in the circumnuclear regions are, on the average a factor 100 larger than those measured in the disks of spiral galaxies, extreme star formation in ultraluminous galaxies will be characterised by a duration about ten times shorter than in the disk (i.e., a few 10^7 years) and a SFR a thousand times that of the disk.

Also, under the GIM, there will be an increase in the lower mass limit of the IMF (M_l), and in the star formation efficiency measured as the fraction of gas mass converted into stars over the whole period of star formation (will correspond to the ϵ^{SB} parameter defined in the equations in Sect. 6.2). According to GIM, the increase in the thermal Jeans mass in the star forming regions will lead to an increase in the lower mass limit in the IMF. On the other hand, the velocity dispersion of the star forming clouds is larger than in the disk as a consequence of processes related to cloud-cloud collisions and turbulence in the circumnuclear regions (Elmegreen 1994). Virialized clouds with a large internal velocity dispersion have a larger binding energy and are therefore more difficult to disrupt (see Elmegreen 1994 for details and references). If the internal velocity dispersion of the star forming clouds is larger, they will be more tightly bound, and more difficult to destroy than under the standard physical conditions of molecular clouds in the disk. Therefore, the total conversion of gas into stars will be about 4%, or larger, if only stars more massive than 3 $M_\odot$ are formed (Elmegreen 1994). This large conversion of gas into stars predicted by the model agrees with our estimated upper limit of 10% for the overall

conversion of gas in stars, in a short lived ($\leq 3\ 10^7$ yr) starburst biased towards massive stars (M_l= 3 $M_\odot$).

Moreover, the GIM predicts an overall gas-to-stars conversion efficiency independent of the gas density, when the whole duration of the starburst is considered. According to the definition of ϵ^{SB} in Sect. 6.2 and considering the GIM predicted dependence of τ_{SF} and SFR on the density, ρ, (Elmegreen 1994)

$$\epsilon^{SB} \propto \frac{\tau_{SF}\ SFR}{M_{H_2}} \propto \frac{\rho^{-0.5}\ \rho^{1.5}}{\rho} = \text{const.}$$

This prediction of GIM is precisely what is obtained from our results: an upper limit in L_{IR}/M_{H_2} independent of Σ_{H_2} implies a uniform upper limit in the gas-to-stars conversion efficiency, ϵ^{SB}, independent of the density.

7. Conclusions

The molecular gas properties and circumnuclear star formation in the nearby nuclear starburst galaxies NGC 2903, NGC 3351 and NGC 3504 have been investigated in detail. The circumnuclear HII regions in the star-forming rings of these galaxies are characterized by an ionized gas mass in the $10^4 - 10^5$ $M_\odot$ range, and by an ionizing flux in the $10^{51} - 10^{52}$ ph s^{-1} range, typical of giant HII regions in external galaxies (GEHRs).

A region approximately $30'' \times 30''$ in size centered on the nucleus of each galaxy has been mapped in the CO 2→1 transition. The CO emission in NGC 3504 indicates the presence of two emitting regions separated by 115 km s^{-1} in velocity and $5''$ (500 pc) spatially, what approximately corresponds to the location of the the inner inner Lindblad resonance. The measured (CO 2→1)/(CO 1→0) integrated intensity ratio for the inner kpc of NGC 3351 is 0.8, in agreement with the empirical average value found for spiral galaxies with a normal metallicity regardless of the presence or the absence of a starburst. Following this general result, a conversion factor χ_{21} between CO 2→1 integrated intensity and molecular hydrogen column density of $\chi_{21} = 0.8^{-1}\chi_{10}$ has been used to convert the measured CO 2→1 emission to molecular gas mass for the three galaxies studied in this paper.

Typical molecular gas mass in the range of $M_{H_2} \approx 10^8 - 10^9$ $M_\odot$ are measured in regions of a few hundred parsecs in size. On the average, the circumnuclear regions of these three starburst galaxies are characterised by a molecular gas surface density $< \Sigma_{H_2} >= 280$ $M_\odot$ pc^{-2}, a global star formation rate $<$ SFR $>= 2$ $M_\odot$ yr^{-1} (for M_l = 3 $M_\odot$ and M_u = 60 $M_\odot$), and a star formation efficiency $<L_{IR}/M_{H_2}>= 21$ $L_\odot$ $M_\odot{}^{-1}$.

The $L_{IR}/M_{H_2} - \Sigma_{H_2}$ relationship covering 4 orders of magnitude in Σ_{H_2} has been studied. Giant Molecular Clouds in the Milky Way, normal spiral galaxies like our Milky Way and M33, nearby starbursts and starbursts with AGNs, and luminous IRAS galaxies have been included in this study.

Nearby circumnuclear starburst galaxies are characterised by an average molecular gas surface density $\Sigma_{H_2} \sim 400$ $M_\odot$ pc^{-2} range, while their star formation efficiency has an average value of 23 $L_\odot$ $M_\odot{}^{-1}$. Their molecular gas surface density and the L_{IR}/M_{H_2} are a factor ~ 3 larger than for GMCs with associated HII regions in the Milky Way. This increase in the SFE is most likely interpreted as an increase by a similar factor on the gas to stars conversion efficiency in molecular clouds in starburst galaxies with respect to GMC with associated HII regions. The overall gas to star conversion in starburst galaxies corresponds to 10% in mass for a short lived starburst ($\tau_{SF} \leq 3\ 10^7$ years) biased towards massive stars ($M_{star} \geq 3\ M_\odot$).

NGC 1068 is considered as the prototype of AGN plus circumnuclear starburst galaxies. For NGC 1068 the IR luminosity associated to the AGN corresponds to ∼50% of the total while the amount of molecular gas in the first ∼100 parsecs around the nucleus is only 3% of the total molecular gas content in the inner region of 1.6 kpc radius. As a consequence, while the SFE associated to the AGN is very large, $(L_{IR}/M_{H_2})^{AGN}$ = 1360 $L_\odot$ $M_\odot{}^{-1}$, the overall observed L_{IR}/M_{H_2} of NGC 1068 is very close (42 $L_\odot$ $M_\odot{}^{-1}$) to that measured in the star formation ring L_{IR}^{SB} $[M_{H_2}^{SB}]^{-1}$= 21 − 44 $L_\odot$ $M_\odot{}^{-1}$.

The star formation efficiency in luminous IRAS galaxies is restricted to the 10 $< L_{IR}/M_{H_2} <$ 100 $L_\odot$ $M_\odot{}^{-1}$ range, and reaches a maximum value of 100 $L_\odot$ $M_\odot{}^{-1}$ for surface densities greater than 10^3 $M_\odot$ pc^{-2}. This upper limit is independent of Σ_{H_2} and extends over more than two orders of magnitude in Σ_{H_2}. This upper limit can only be reached in luminous infrared galaxies, like Mrk 231, if an AGN contributes significantly to the infrared luminosity.

As for NGC 1068, the $L_{IR}/M_{H_2} - \Sigma_{H_2}$ relationship observed in nearby Seyferts with starbursts, and luminous IRAS galaxies is explained as a combination of massive star formation in the circumnuclear regions of these galaxies with the contribution of an AGN in the center of the galaxy. Under this model, most of the molecular gas mass is directly associated to the circumnuclear star forming regions while the AGN contributes to 10%−75% of the global IR luminosity, depending on the galaxy. In this scenario, the infrared luminosity of galaxies with observed L_{IR}/M_{H_2} in the 10 to 30 $L_\odot$ $M_\odot{}^{-1}$ range is dominated by the circumnuclear star formation alone. Nearby examples of this situation are NGC 3079 or NGC 3227. The infrared luminosity in those galaxies with L_{IR}/M_{H_2} in the 30–100 $L_\odot$ $M_\odot{}^{-1}$ range is increasingly dominated by the central AGN. Examples of this situation are NGC 1068, NGC 7469, or Mrk 231 where the AGN contribution would be 50% to 80% of the global IR luminosity.

Acknowledgements. We thank the IRAM staff for their help during the observations at Pico Veleta. We also thank R. Bachiller for critical reading of part of the manuscript. D.P.O. acknowledges the support of the Spanish Council for Research and Technology (DGYCIT) under grants PB90-0182 and PB-0252. P.P. acknowledges partial support by the Spanish DGICYT under projects PB90-408 and PB93-0048 and by the Collaborative Visitor Program at the STScI.

References

Alloin, D., Nieto, J.L. 1982, A&AS, 50, 491
Balzano, V.A. 1983, ApJ, 268, 602
Barnes, J.E., Hernquist, L.E. 1991, ApJ, 370, L65
Braine, J., Combes, F. 1992, A&A, 264, 433

Braine, J., Combes, F., Casoli, F. et al., 1993, A&AS, 97, 887
Buta, R., Crocker, D.A. 1993, AJ, 105, 1344
Colina, L., Lipari, S., Macchetto, F.D. 1991, ApJ, 379, 113
Colina, L., Pérez-Olea, D. 1992, MNRAS, 259, 709
Colina, L., Pérez-Olea, D. 1995, MNRAS, 277, 845
Combes, F. 1991, in IAU Symp. 146 in *Dynamics of Galaxies and their Molecular Cloud Distributions*, Ed.: F. Combes & F. Casoli, p. 225, Kluwer
de Juan, L., Colina, L., & Golombek, D. 1996, A&A, 305, 775
Devereux, N., Kenney, J.D.P., Young, J.S. 1992, AJ, 103, 784
Dickman, R.L., Snell, R.L., Schloerb, F.F. 1986, ApJ, 309, 326
Doyon, R., Joseph, R.D., Wright, G.S. 1994, ApJ, 421, 101
Eckart, A., Downes, D., Genzel, R. et al., 1990, ApJ, 348, 434
Elmegreen, B. 1994, in *Violent Star Formation from 30 Dor to QSOs* Ed.: G. Tenorio Tagle, University of Cambridge Press, p. 220
Fullmer, L., Lonsdale, C. 1989, *Cataloged Galaxies and Quasars observed in the IRAS Survey*, Version 2, Jet Propulsion Laboratory
García-Burillo, S., Guélin, M., Cernicharo, J. 1993, A&A, 274, 123
Gerin, M., Nakai, N., Combes, F. 1988, A&A, 203, 44
Ghosh, S.K., Verma, R.P., Rengarajan, T.N., Saraiya, H.Y. 1993, ApJSS, 86, 401
González-Delgado, R.M. 1995, Doctoral Dissertation, University of La Laguna (Spain)
González-Delgado, R.M., Pérez, E., Díaz, A.E. et al., 1995, ApJ, 439, 604
Grosbol, P. 1985, A&AS, 60, 261
Heckman, T.M. 1991, in *Massive stars in Starbursts*, Eds.: C. Leitherer, N.R. Walborn, T. M. Heckman, C.A. Norman, Cambridge Univ. Press
Heckman, T.M., Blitz, L., Wilson, A.S., Armus, L. 1989, ApJ, 342, 735
Heckman, T.M., van Breugel, W., Miley, G.K., Butcher, H.R. 1983, AJ, 88, 1077
Hernquist, L. 1989, Nat, 340, 687
Ho, P.T.P., Beck, S.C., Turner, J.L. 1990, ApJ, 349, 57
Hummel, E., van der Hulst, J., Keel, W.C. 1987, A&A, 172, 32
Jackson, J.M., Snell, R.L., Ho, P.T.P., Barret, A.H. 1989, ApJ, 337, 680
Jackson, J.M., Eckart, A., Cameron, M. et al., 1991, ApJ, 375, 105
Kenney, J.D.P., Carlstrom, J.E., Young, J.S. 1993, ApJ, 418, 687 (KCY)
Kenney, J.D.P., Wilson, C.D., Scoville, N.Z., Devereux, N.A., Young J.S. 1992, ApJ, 395, L79
Kennicutt, R.C. 1991 in *Massive Stars in Starbursts*, Eds.: C. Leitherer, N.R. Walborn, T.M. Heckman, C.A. Norman, Cambridge Univ. Press, p. 157
Kjeldsen, H. 1990, Test of the Stockholm CCD camera mounted on the NOT adaptor
Macchetto, F.D., Colina, L., Golombek, D., Perryman, M.A.C., di Serego Alighieri, S. 1991, ApJ, 356, 389
Maloney, P. 1990, in *The Interstellar Medium in Galaxies*, ed. by H.A. Thronson & J.M. Shull, Kluwer
Noguchi, M. 1988, A&A, 201, 37
Perault, M. 1987, Thése d'Etat, Université Paris 7. pp 165-208
Pérez-Olea, D., Colina, L. 1995, MNRAS, 277, 857
Planesas, P., Gómez-González, J., Martín-Pintado, J. 1989, A&A, 216, 1
Planesas, P., Mirabel, I.F., Sanders, D.B. 1991, ApJ, 370, 172
Planesas, P., Scoville, N., Myers, S.T. 1991, ApJ, 369, 364
Puxley, P.J., Hawarden, T.G., Mountain, C.M. 1988, MNRAS, 234, 29P
Puxley, P.J., Hawarden, T.G., Mountain, C.M. 1990, ApJ, 364, 77
Rice, W., Boulanger, F., Viallefond, F., Soifer, B.T., Freedman, W.L. 1990, ApJ, 358, 418
Rowan-Robinson, M., Crawford, J. 1989, MNRAS, 238, 523
Saikia, D.J., Pedlar, A., Unger, S.W., Axon, D.J. 1994 MNRAS, 270, 46
Sandage, A., Tammann, G. 1987 A Revised Shapley-Ames Catalog of Bright Galaxies, Carnagie Institution of Washington (Washington, DC)
Sanders, D.B. Scoville, N.Z., Sargent, A.I., Soifer, B.T. 1988 ApJ, 324, L55
Sanders, D.B., Scoville, N.Z., Soifer, B.T. 1988, ApJ, 335, L1
Sanders, D.B., Scoville, N.Z., Soifer, B.T. 1991, ApJ, 370, 158
Sargent, A.I., Scoville, N.Z. 1991, ApJ, 366, L1
Scoville, N.Z., Good, J.C. 1989, ApJ, 339, 149
Scoville, N.Z., Sanders, D.B., Clemens, D.P. 1986, ApJ, 310, L77
Scoville, N.Z., Sanders, D.B., Sargent, A.I., Soifer, B.T., Tinney, C.G. 1989, ApJ, 345, L25
Scoville, N.Z., Sargent, A.I., Sanders, D.B., Soifer, B.T. 1991, ApJ, 366, L5
Scoville, N.Z., Soifer, B.T. 1991 in *Massive Stars in Starbursts*, Eds.: C. Leitherer, N.R. Walborn, T.M. Heckman, C.A. Norman, Cambridge Univ. Press, p. 233
Scoville, N.Z., Yun, M.N., Clemens, D.P., Sanders, D.B., Waller, W.H. 1987, ApJS 63, 821
Sersic, J.L., Pastoriza, M. 1967, PASP 79, 152
Smith, J. 1982, ApJ, 261, 463
Solomon, P.M., Rivolo, A.R., Barrett, J.W., Yahil, A. 1987, ApJ, 319, 730
Stanford, S.A., Sargent, A.I., Sanders, D.B., Scoville, N.Z. 1990, ApJ, 349, 492
Stauffer, J.R. 1982, ApJS, 50, 517
Taniguchi, Y., Nakai, N., Kameya, O. 1991, in IAU Symp. 146 on *Dynamics of Galaxies and their Molecular Cloud Distributions*, Ed.: F. Combes & F. Casoli, Kluwer
Telesco, C.M., Becklin, E.E., Wynn-Williams, C.G., Harper, D.A. 1984 ApJ, 282, 427
Telesco, C.M., Dressel, L.L., Wolstencroft, R.D. 1993, ApJ, 414, 120
Ulvestad, J.S., Wilson, A.S., Sramek, R.A. 1981, ApJ, 247, 419
de Vaucouleurs, G., de Vaucouleurs, A., Corwin, H.G. et al., 1991, in *Third Reference Catalogue of Bright Galaxies*, Springer-Verlag
Wang, Z., Scoville, N.Z., Sanders, D.B. 1991, ApJ, 368, 112
Wilson, A.S., Helfer, T.T., Haniff, C.A., Ward, M.J. 1991, ApJ, 381, 79
Wilson, C.D., Scoville, N.Z. 1989, ApJ, 347, 743
Wynn-Williams, C.G., Becklin, E.E. 1985, ApJ, 290, 108
Young, J.S., Clausen, M.J., Kleinmann, S.G., Rubin, V.C., Scoville, N.Z. 1988, ApJ, 331, L81
Young, J.S., Claussen, M.J., Scoville, N.Z. 1988, ApJ, 324, 115
Young, J.S., Xie, S., Kenney, J.D.P., Rice, W.L. 1989, ApJS, 70, 699

This article was processed by the author using Springer-Verlag LaTeX A&A style file *L-AA* version 3.